AALBORG UNIVERSITY

DENMARK

An Experimental Study of the Modal Parameters of a Damaged Cantilever

Rytter, A.; Brincker, Rune; Kirkegaard, Poul Henning

Link to publication from Aalborg University

FRACTURE AND DYNAMICS
PAPER NO. 37

A. RYTTER, R. BRINCKER & P. H. KIRKEGAARD
AN EXPERIMENTAL STUDY OF THE MODAL PARAMETERS OF A
DAMAGED CANTILEVER

INSTITUTTET FOR BYGNINGSTEKNIK
DEPT. OF BUILDING TECHNOLOGY AND STRUCTURAL ENGINEERING
AALBORG UNIVERSITETSCENTER • AUC • AALBORG • DANMARK

A. RYTTER, R. BRINCKER & P. H. KIRKEGAARD
AN EXPERIMENTAL STUDY OF THE MODAL PARAMETERS OF A DAMAGED CANTILEVER

AN EXPERIMENTAL STUDY OF THE MODAL PARAMETERS OF A DAMAGED CANTILEVER

A. RYTTER

Rambøll, Hannemann & Højlund, Kjærulfsgade 2, DK-9400 Nørresundby, Denmark

R. BRINCKER AND P. H. KIRKEGAARD

Department of Building Technology and Structural Engineering, University of Aalborg,
DK-9000 Aalborg, Denmark

ABSTRACT

The introduction of a crack in a structure will cause a local change in stiffness and damping capacity. The local change in stiffness, normally a decrease, will lead to a change of the natural frequencies of the structure and a discontinuity in the mode shapes. This report contains a presentation of results from experimental tests with six hollow section steel cantilevers containing a fatigue crack introduced from a narrow laser cut slot. The modal parameters have been identified for different size and location of a crack. The modal parameters have been estimated by mean of frequency domain and time domain system identification techniques. A short description of these system identification methods is given.

PREFACE

The present report *An Experimental Study of the Modal Parameters of a Damaged Cantilever* has been prepared as a part of the research project *Integrated Experimental and Analytical Investigations of the Dynamic Behaviour of Offshore Structures* at the Department of Building Technology and Structural Engineering, University of Aalborg during the period from April 1991 to June 1992.

The figures has been carried out by draugthsman Mrs. Norma Hornung. Her careful work is greatly appreciated.

Thanks are also given to the staff in the laboratory, led by engineer assistant Mr. Henning Andersen, for help during the performance of the experimental tests.

Aalborg, Denmark   Poul Henning Kirkegaard
October, 1992   Rune Brincker
                                                Anders Rytter

CONTENTS

APPENDIX

1. INTRODUCTION

The introduction of damage like e.g. a crack in a steel structure will cause a local change in stiffness and damping capacity. The local change in stiffness will lead to a change of the natural frequencies of the structure and a discontinuity in the mode shapes. The stiffness will normally decrease when a crack is introduced. This means that the natural frequencies will either decrease or remain unchanged depending on the location of the crack. The increase in damping is due to the fact that the structure contains a yielding zone at the crack tip. This means that energy will be dissipated in this zone during a load cycle, which implies an increase in the damping capacity of the structure.

The above-mentioned effects of a crack means that the measurement of natural frequencies, mode shapes and damping ratios during the lifetime of a structure can be used for detection of damage in the structure.

This paper contains a presentation of results from experimental tests with six hollow section steel cantilevers containing a fatigue crack. The cracks were initiated from the ends of small narrow cut slots. The main purpose of the tests was to obtain experimental sets of data (modal parameters belonging to a certain crack length), which can form the basis for an evaluation of different damage detection methods (see Rytter [1]). Further the results will be used to calibrate/verify an analytically model for the local decrease in stiffness of a hollow section profile as function of crack length (see Rytter et al. [2]).

Section 2 of this report contains a description of the experimental setup complemented with a review of some the practical problems, which cropped up before and during the tests.

The modal parameters have been estimated for different size and two different locations of a crack by mean of frequency domain and time domain system identification techniques. A short description of these system identification methods and some methods to give a qualitative indication of damage is given in section 3.

The main results are presented in section 4, whereas appendices C-H contain a more detailed presentation of the results.

Finally a discussion and a conclusion are given in section 5.

2. EXPERIMENTAL ARRANGEMENT

The experimental tests were performed on six different hollow section cantilevers made of steel. The six beams will in the remaining part of this report be referred to as B1, B2, B3, B4, B5 and B6 respectively.

The most important sectional parameters and material properties are shown in figure 1.
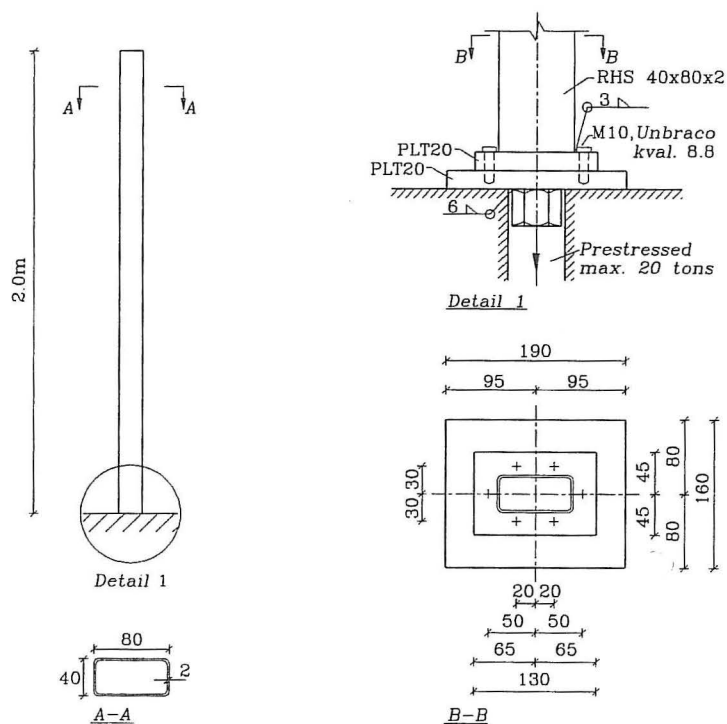
Measurements in mm

Figure 1 Test beams.

As mentioned earlier the aim of the tests was to obtain experimental estimates for the

modal parameters for different size and location of a true fatigue crack.

In many tests concerning the same problem saw cuts have been used to emulate fatigue cracks (see e.g. Wendtland [3] and Ju and Mimovich [4]). However this kind of tests will often lead to a wrong picture of the relationship between the crack length and the changes in the modal parameters. This due to the fact that the changes in the modal parameters depend on the width of the crack/cut too (see e.g. Cawley and Ray [5]). Further the nonlinear effects due to opening and closing of a fatigue crack will be missed in tests, where saw cuts are used to emulated fatigue cracks. Therefor small narrow laser cuts (width $\approx$ 0.15 mm) have been used to initiated the fatigue cracks in the six test beams (see figure 3).

The profile of fatigue cracks will often be irregular (see figure 2), which means that it some times can be difficult to get a reliable measure of the crack depth/length during fatigue tests. To avoid this the wall thickness of the six test beams has been chosen as 2 mm. Thereby it should be possible to measure the crack length at the outside of the profiles.

The crack lengths given in this report are referred to the centerline of the profile. The crack length on each side of the centerline (x-axis) has been measured and reported (see figure 3) to avoid for misunderstandings in cases with skew crack growth ($a_l \neq a_r$). The latter occurred, as it can be seen from appendices C-H, in more or less extent for all six test beams.
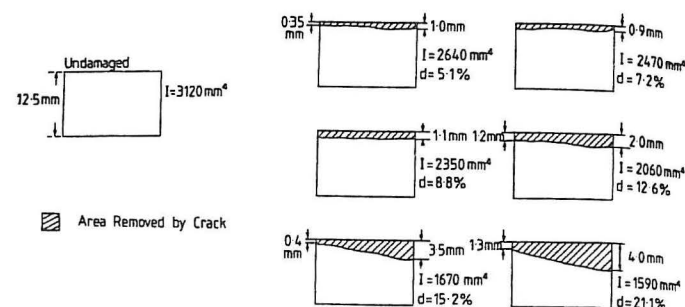
Figure 2 Profile of fatigue cracks (Cawley and Ray [5])

The cracks in beam B1-B3 and B4-B6 were initiated at $z = 1.0$ m and $z = 0.1$ m, respectively (see figure 3). The fatigue cracks were initiated and developed by attaching
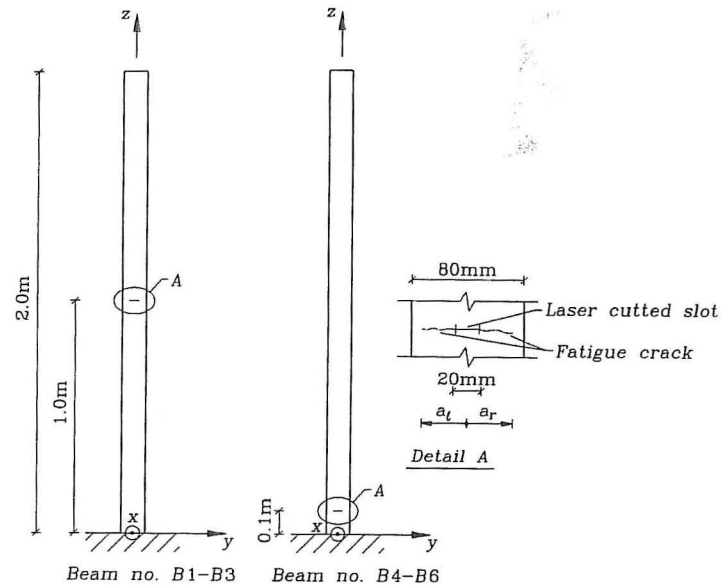
Figure 3 Crack locations.

a sinus-varying load to the beams by mean of a shaker (see figure 4). The frequency of the sinus was either the actual first or second bending natural frequency. The use of the second natural frequency gave a fast crack growth. However the tests showed that the use of this frequency increased the risk for skew crack growth and fatigue cracks in the weld at the fixture considerable.

The tests on beam B1 and B2 were interrupted due to fatigue cracks in the fixture weld. Therefore a reinforcement arrangement was mounted during the fatigue of beam B3, B5 and B6. The fatigue of beam B4 was performed at the first natural frequency without reinforcement. No unwanted fatigue cracks were initiated in this beam.

The crack lengths were measured by mean of either a microscope mounted on an
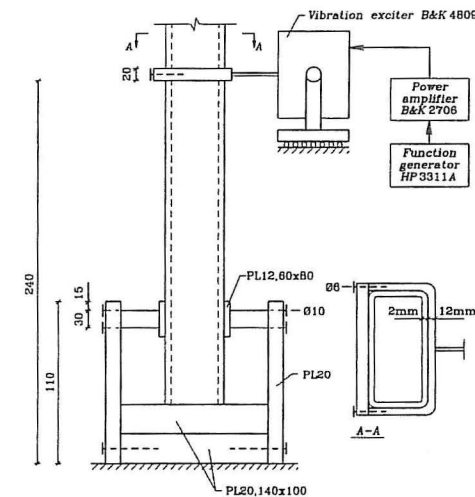
Figure 4 Arrangement for fatigue

electrical measurement rail or a Vernier gauge and a magnifying glass. The actual measurement method is stated in appendices C-H.

A lumped mass of 0.377 kg has been attached to beam B1 and B6 in two different positions (see figure 5) for certain crack lengths (see appendix C and H). The results from the measurement performed with these configurations will be used to test the applicability and effectiveness of the damage detection methods in Rytter [1].

2.1. FREE DECAY TESTS

The basic instrumentation for the free decay tests is shown in figure 6. The free decays of the beams were introduced by removing a well-defined static load from the beam momentary.

The sample frequency was set to 317,85 Hz $\approx$ 28$\cdot f_1^{virgin}$, where f_1^{virgin} is the first natural
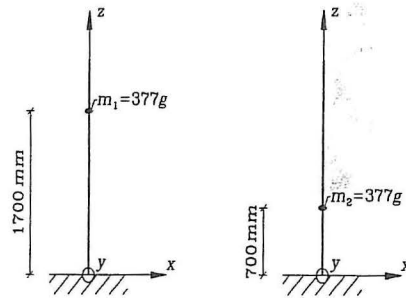
Figure 5 Positions of lumped masses.
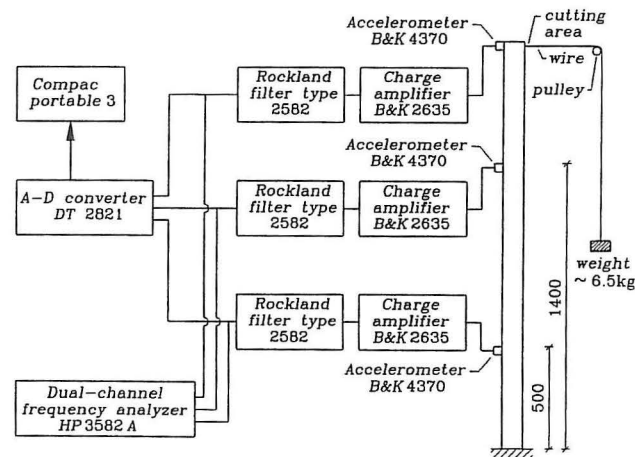
Figure 6 Instrumentation for free decay tests.

frequency at the virgin state.

The analog filters shown in figure 6 were used as low pass filter (cut off at 20 Hz)

during the tests on beam B4 only. Digital elliptic filters (see appendix B) were used on the measurements from the other five beams. In the latter cases the raw data were stored on the computer for subsequent analysis.

2.2. MODAL ANALYSIS

The instrumentation used in connection with the performed experimental modal analysis is shown in figure 7.
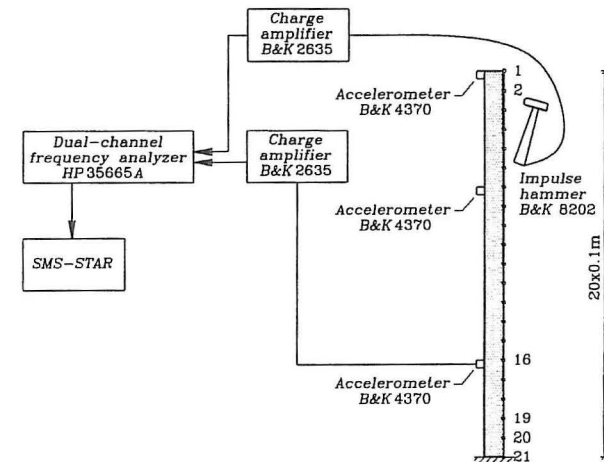
Figure 7 Instrumentation for modal analysis.

The modal analysis included excitation by an impact hammer in 20 equally spaced points. Point 16 was chosen as the driving point.

Dummy accelerometers were mounted in point 1 and 7 respectively to obtain results, which are directly comparable with the results from the free decay tests.

3. SYSTEM IDENTIFICATION

The aim of this section is to give a short description of those system identification methods, which have been used to obtain estimates for the modal parameters from the test results. Further there will given a short description of some methods, which can be used to give a qualitative indication of damage in a structure.

3.1. PERIODS OF ZERO-CROSSINGS

An estimate of the damped natural frequency $\hat{f}_{nd}$ is determined from the interval between zero-crossings in a free decay, as shown in figure 8 and equation (1).

$$\hat{f}_{nd} = \frac{1}{N_p}\sum_{i=1}^{N_p} \frac{1}{T_i^+ + T_i^-} \qquad (1)$$

where N_p is the number of periods, T_i^+ is the duration of the $i'th$ positive half-cycle and T_i^- is the duration of the $i'th$ negative half-cycle.

An estimate for the natural frequency $\hat{f}_n$ is given as

$$\hat{f}_n = \hat{f}_{nd}\sqrt{1-\hat{\zeta}_n^2} \qquad (2)$$

where $\hat{\zeta}_n$ is an estimate for the modal damping ratio (see section 3.2).

T_i^+ and T_i^- will only be equal if the beam is linear for all amplitudes, which means it has to be either intact or contain a symmetric double-sided open crack. The latter will rarely occur for a cracked beam, which implies that T_i^+ and T_i^- might be used as damage indicators (see figure 9). Further it shall be noticed that T_i^+ and T_i^- are the damped natural half periods, which means that they might be used to indicate amplitude depending damping.

During the free decay tests the third and fourth natural frequency were determined as resonance peak frequencies on FRF's. The FRF's were calculated by mean of the HP3582A dual channel analyzer. Even though the zoom facilities of the analyzer were used, the natural frequencies were determined with a limited accuracy.
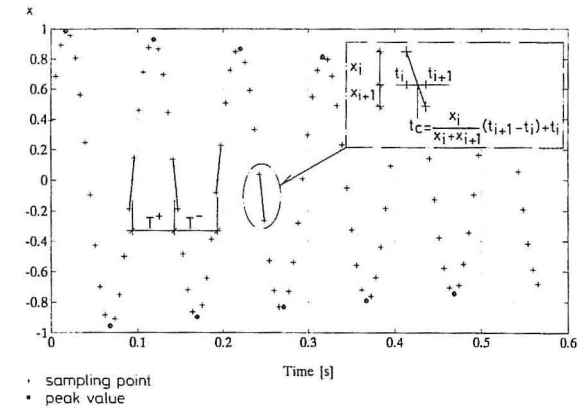
Figure 8
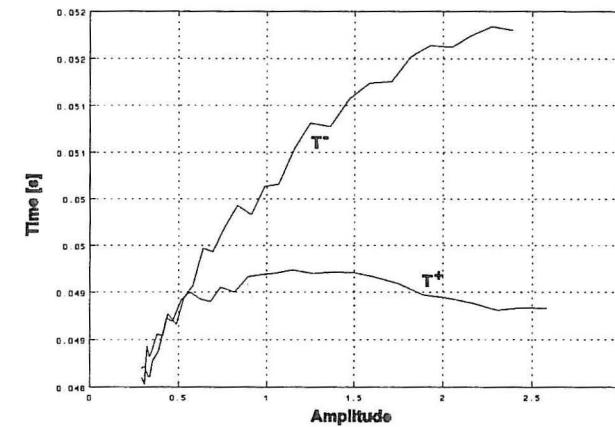
Figure 9 Positive and negative half periods versus amplitude, beam B4, series O2.

3.2. DAMPING

The logarithmic decrement δ of a linear and viscously damped system is defined by in which X_1 is the value of the first extreme and X_i is the value of the $i'th$ extreme

$$\delta = \frac{2}{i-1} \ln(\frac{|X_1|}{|X_i|}) \leftrightarrow \ln(|X_i|) = -\frac{\delta}{2}(i-1) + \ln(|X_1|) \qquad (3)$$

(either positive or negative) of a free decay. The extremes were found from the sampled time series as shown in figure 8.

An estimate $\hat{\delta}$ for the logarithmic decrement and of $\hat{X}_i$ can thus be determined through a linear regression on $\ln(|X_i|)$ and i. An estimate for the damping ratio is then given as

$$\hat{\zeta}_n = \frac{\hat{\delta}}{\sqrt{\hat{\delta}^2 + 4\pi^2}} \qquad (4)$$

A similar technique can be used to give estimates for the amplitude X of the free decay and the damping ratio ζ if an estimate $\hat{f}_n$ for the natural frequency is known. In this case the linear relationship between $\ln(|X_i|)$ and t_i is given by

$$\ln(|X_i|) = -\hat{\zeta}_n 2\pi \hat{f}_n t_i + \ln(X) \qquad (5)$$

The latter methods have been used to establish good start estimates for the system parameter in connection with the performed curve fits on free decays (see section 3.4).

Energy will be dissipated in the yielding zone at the tip of a fatigue crack, which means that the damping capacity of the structure will increase. However the increase will often depends on the amplitude of the vibration, which makes the system non linear. This mean that equation (3) no longer will be valid. Thus a plot of the logarithmic value of the extreme values $\ln(|X_i|)$ against the peak number i can be used to indicate damage, as shown in figure 10 .

3.3. MODE SHAPE RATIOS

The displacement in two measurement points during a free decay of a linear and viscously damped system are related to each other in the following way

$$x_2(t) = \frac{\Phi_2}{\Phi_1} x_1(t) \qquad (6)$$

where $x_i(t)$ is the response and Φ_i is the modal coordinate at the $i'th$ measurement point.
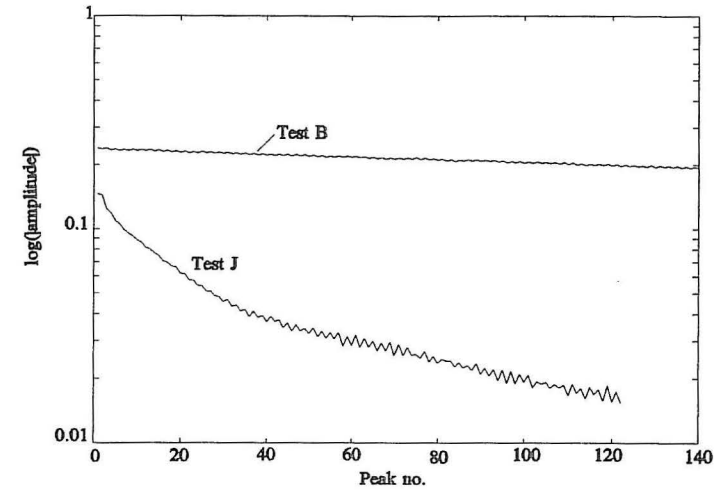
Figure 10 Peak values versus peak no., beam B6, Test B and J.

The ratio between the modal coordinate of two measurement points can thus be found through a linear regression between the sampled time series from the two points (see figure 11).
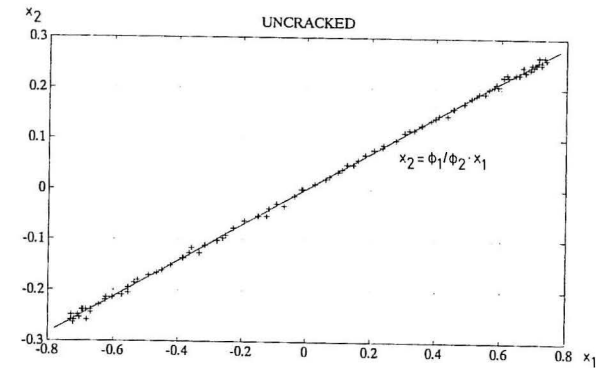
Figure 11 Displacement in two measurement points, uncracked case.

The formula given in equation (6) is only valid, when the beam behaves linear for all amplitudes. This means that plots like the one in figure 11 can be used as damage indicators, as illustrated in figure 12 for a beam containing a one-sided crack, which is open and closed by turn and placed between the two measurement points.
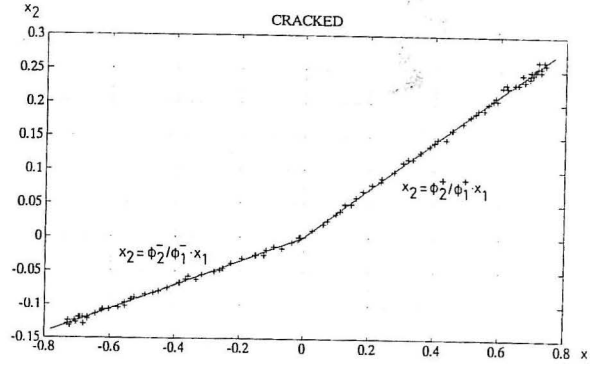
Figure 12 Displacement in two measurement points, cracked case.

3.4. CURVE FIT ON FREE DECAYS

A free decay $x(t)$ of a linear and viscously damped system of one degree of freedom is given by

$$x(t_i|\overline{\theta}) = X e^{-2\pi\zeta_n f_n t_i} \cos(\sqrt{1-\zeta_n^2}\, 2\pi f_n t_i + \phi) \tag{7}$$

in which X is the amplitude, ζ_n is the modal damping ratio, f_n is the natural frequency and ϕ is the phase. These four parameters (X, ζ_n, f_n, ϕ) make up the system vector $\overline{\theta}$.

Estimates $\hat{\theta}_N$ for the elements in $\overline{\theta}$ can be determined from a measured discrete time series $x(t_i)$ of N points by minimizing the following sum of square errors

$$V_N(\overline{\theta}) = \frac{1}{N} \sum_{i=1}^{N} \frac{1}{2}\, \epsilon^2(t_i, \overline{\theta}) \tag{8}$$

in which

$$\epsilon(t_i, \overline{\theta}) = x(t_i) - \hat{x}(t_i|\overline{\theta}) \tag{9}$$

An asymptotic estimate for the covariance matrix of the system parameters estimated by mean of (8) is given by (see Ljung [6])

$$Cov\,\hat{\theta}_N \sim \frac{1}{N}\overline{P}_\theta \tag{10}$$

$$\overline{P}_\theta \approx \hat{P}_N = \hat{\lambda}_N [\frac{1}{N}\sum_{i=1}^{N} \overline{\Psi}(t_i, \hat{\theta}_N)\, \overline{\Psi}(t_i, \hat{\theta}_N)]^{-1} \tag{11}$$

$$\hat{\lambda}_N = \frac{1}{N} \sum_{i=1}^{N} \epsilon^2(t_i, \hat{\theta}_N) \tag{12}$$

in which $\overline{\Psi}$ is the gradient of $\hat{x}(t_i|\overline{\theta})$ with respect to $\overline{\theta}$. The expressions given in (10)-(12) are in principle only valid in connection with identification of linear system loaded with stationary white noise. However, a simulation study has shown that the expressions give reasonable estimates of the variance of the system parameters estimated through curve fitting on free decays of lightly damped systems (see appendix 1).

The identification of the natural frequencies f_1 and f_2, the modal damping ratios ζ_1 and ζ_2 and the relative modal coordinates in the measurement point of the two lower modes from free decays is based on a minimization for each measurement point of the error function $V_N(\overline{\theta})$ given in equation (13).

$$V_N(X_{ji}, \zeta_i, f_i, \phi_j, x_{zero}) = \sum_{k=1}^{N} (x^*(t_k) - X_{ji} e^{-2\pi\zeta_i f_i t_k}\cos(\sqrt{1-\zeta_i^2}\, 2\pi f_i t_k + \phi_j) - x_{zero})^2 \tag{13}$$

where $x^*(t_k)$ is the filtered signal (see section 2.1), X_{ji} is the amplitude at measurement point j, f_s is the sampling frequency and ϕ_j is the phase. The x_{zero}-term has been included to avoid for a possible DC-signal.

The minimization of (13) have been performed by mean of the m-file CONSTR in the optimization toolbox for MATLAB (see [7]).

The ratio between the modal coordinates of two measurement points is calculated as

$$\frac{\Phi_{ji}}{\Phi_{li}} = \frac{X_{ji}}{X_{li}} \frac{sign(\sin(\phi_j))}{sign(\sin(\phi_l))} \tag{14}$$

where Φ_{ji} is the modal coordinate of mode i at measurement point j.

The estimates of $f_{i,k}$ and $\zeta_{i,k}$ from each of the N_p measurement points are combined in the following way

$$f_i = \frac{\sum_{k=1}^{N_p} \frac{f_{i,k}}{\sigma^2_{f_i,k}}}{\sum_{k=1}^{N_p} \sigma^{-2}_{f_i,k}} \tag{15}$$

$$\zeta_i = \frac{\sum_{k=1}^{N_p} \frac{\zeta_{i,k}}{\sigma^2_{\zeta_i,k}}}{\sum_{k=1}^{N_p} \sigma^{-2}_{\zeta_i,k}} \tag{16}$$

where $\sigma^2_{f_i,k}$ and $\sigma^2_{\zeta_i,k}$ are the variance of the estimates of f_i and ζ_i found from measurements in point k.

The standard deviation of f_i and ζ_i is calculated from

$$\sigma^{-2}_{f_i} = \sum_{k=1}^{N_p} \sigma^{-2}_{f_i,k} \tag{17}$$

$$\sigma^{-2}_{\zeta_i} = \sum_{k=1}^{N_p} \sigma^{-2}_{\zeta_i,k} \tag{18}$$

3.5. MODAL ANALYSIS

Estimates for the modal parameters of a linear and viscously damped system can be obtained through an experimental modal analysis.

The basic idea in an experimental modal analysis is to perform a curve fit on a set

frequency response functions $H_{ij}(f)$ given by

$$H_{ij}(f) = \frac{G_{x_i x_i}(f)}{G_{F_j x_i}(f)} \tag{19}$$

where $G_{x_i x_i}(f)$ is the autospectral density function of the response in point i and $G_{F_j x_i}(f)$ is the cross spectral density function between the load in point j and the response in point i.

The frequency response function shall be obtained in one of the following two ways

- a shaker is attached to the structure in a fixed point and an accelerometer is successively moved around to different positions on the structure

- an accelerometer is attached to the structure in a fixed point and the structure is excited in different positions by mean of an impact hammer.

The latter method has been used in connection with the test presented in this report, because a shaker could not be attached without disturbing the structure.

The modal analysis has been performed by mean of the STAR*Struct*-software from SMS (see SMS [8]). A more detailed description of experimental modal analysis can be found in several text books (see e.g. Ewins [9]).

3.6. PHASE-PLAN PLOTS

A phase-plan plot of a free vibration of a linear undamped one degree of freedom system will be an ellipse, as shown in figure 13A. A similar plot for a piecewise-linear system will consist of fragments of different ellipse, as shown in figure 13B.

The introduction of a crack will typical make a structure piecewise-linear. This means that phase-plan plots can be used to reveal the existence cracks. Figure 14 shows that this method is applicable for damped structures with more than one degree of freedom.
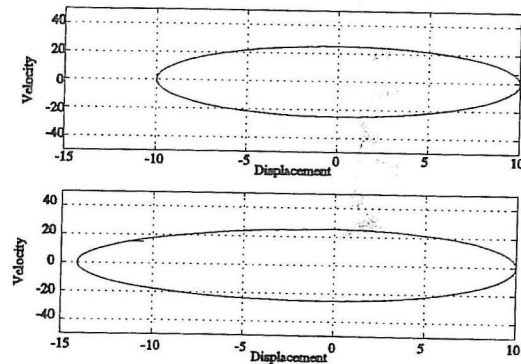
Figure 13 Phase-plan plot for 1 DOF systems.
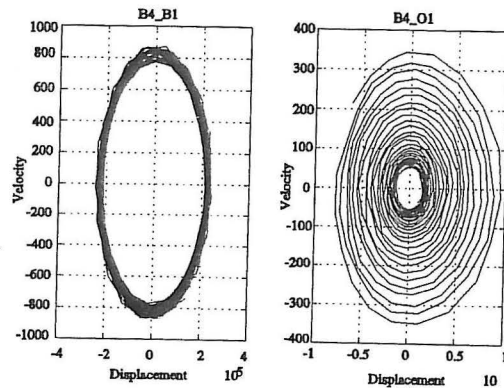
Figure 14 Phase-plan plots. Beam no. 4 case B4_B1 and B4_O1.

3.7. NON EXPECTED RESONANCE FREQUENCIES

The HP3582A frequency analyzer was currently used during the free decay tests to give estimates of the second, third and fourth natural frequency.

This on-line use of the analyzer lead indirectly to the exposure of the fatigue crack at the fixture of beam no. 1 and 2. The asymmetric nature of these cracks lead namely to a change in the orientation of the principal axis of vibration. Therefore the auto spectral density functions of the vibration in the x-direction began to contain resonance frequency peaks at the natural frequencies of vibrations in the y-direction (see figure 15). This

means that a currently control of spectra or FRF of a dynamic loaded structure in principle can be used as a simple method to give an indication of damage at an early stage.
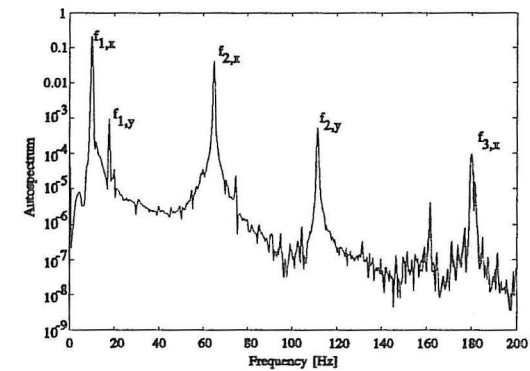
Figure 15 Auto spectral density function, beam B1 , test G.

4. RESULTS

This section contains a presentation of the main result, while a detailed presentation of the results for the single beams is given in appendices C-H.

Figure 16 Symbols used in the subsequent figures

4.1. NATURAL FREQUENCIES

The first natural frequency f_1 is as expected more sensitive to damage at $z = 0.1$ m than at $z = 1.0$ m (see figure 17 and figure 18). The curvature of the first mode shape is greater at $z = 0.1$ m than at $z = 1.0$ m, which makes the beam more sensitive to a certain change in bending stiffness at the lower position. Figure 17A reveals that the earlier mentioned fatigue crack at the fixture of B1 was initiated at the start of the test series and propagated during all the fatigue sessions. Whereas the similar crack in B2 was first initiated during the fatigue loading between the last two tests (test E and F, see appendix D) The course of the drop in f_1 of B5 and B6 for $a_{tot} \in [80\,mm; 120\,mm]$ is different from the similar curve for B4. This due to skew crack growth in B5 and B6 (see appendices G and H), while the crack growth in B4 was almost symmetrical (see appendix F).
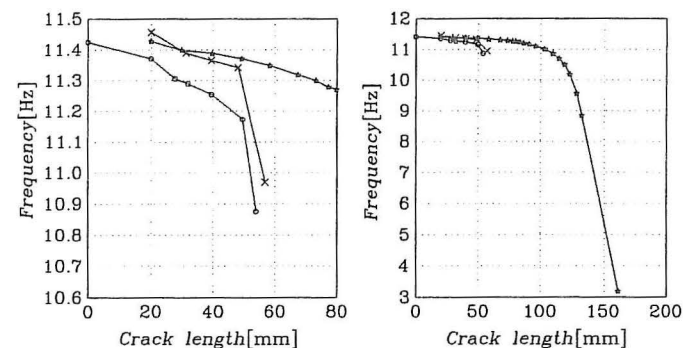
Figure 17 1st natural frequency, beam B1-B3
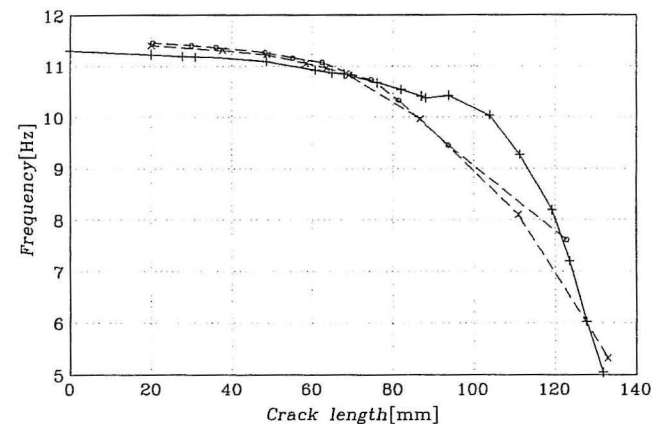
Figure 18 1st natural frequency, beam B4-B6.

Figure 19 reveals that f_2 also is more sensitive to damage at z = 0.1 m than at z = 1.0 m. However the difference in sensitivity is only noticeable for $a_{tot} > 80mm$ corresponding to that the crack tips are located in the webs of the profile. The conclusion about the fatigue cracks at the fixture of B1 and B2 are confirmed by the course in f_2 for these two beams.
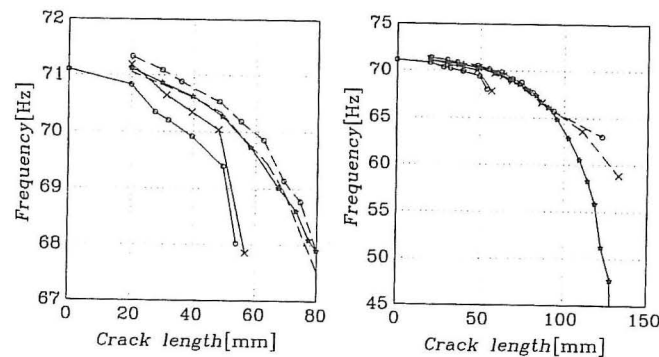
Figure 19 2nd natural frequency, beam B1-B3, B5 and B6

Figure 20 shows that f_3 is very sensitive to damage at z = 0.1 m. Whereas it is almost insensitive to damage at z = 1.0 m. The latter is due to that the third mode shape has a node at z ≈ 1.0 m, which means that curvature is very small. The presence of the above mentioned fatigue cracks at the fixture of B1 and B2 can be seen from figure 20.

The obtained estimated values for f_4 are more scattered for $a_{tot} < 60mm$ than the similar estimates for f_1, f_2 and f_3 (see figure 21). The relatively big band width (BW = 2 Hz) used on the HP3582A-analyzer and a low signal to noise ratio are probably the main reasons for this scattering. Estimates for f_4 for $a_{tot} > 60mm$ are obtained for B3 and B6. The drop in f_4 of B3 is about 60 Hz, which corresponds to approximately 15 %. This big drop is due that the fourth mode shape has a local maximum in curvature nearby z = 1.0 m. Whereas the curvature is nearly zero at z = 0.1 m, which lead to an almost constant value of f_4 for B6 during the whole test series.
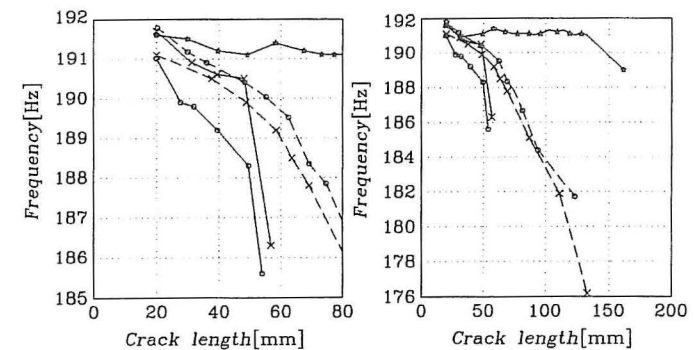
Figure 20 3rd natural frequency, beam B1-B3, B5 and B6.
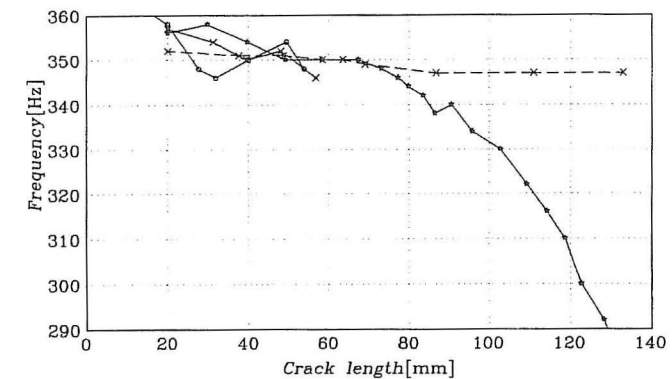
Figure 21 4th natural frequency, beam B1-B3 and B6.

4.2. MODAL DAMPING RATIOS

Figure 21 shows a certain scatter in the estimated values of ζ_1 for $a_{tot} < 80mm$, which makes is almost impossible to distinguish changes due to damage from the randomness

of the estimated values. The low damping and the limit number of data points are the primary reasons to the observed scatter. However it is clear that the fatigue crack at the fixture of B1 causes an increase in ζ_1 on about 400%. Further the ζ_1-curve for B4 shows a similar trend. The trend of the development of ζ_1 with growing a_{tot} is an increase on about 100% for B3 and about 200% for B5 and B6.
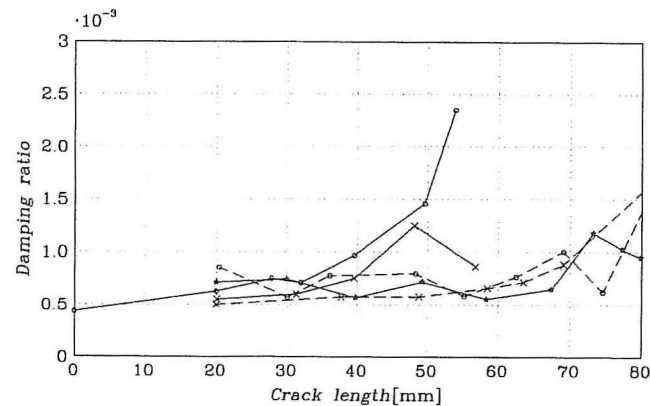
Figure 22 1st modal damping ratio

The above mentioned trend and differences between the estimated values of ζ_1 for B3-B6 are confirmed in figure 23, which shows the ζ_1-curves for values of $a_{tot} > 80 mm$ too. ζ_1 of B4 is increased with a factor about 70 for $a_{tot} = 120 mm$ and drop for the last three measurements. This drop is due to the amplitude dependency of the damping (see figure 10), because of that the amplitude in the free decays was lowered successively in these three test for practical reasons.

The use of a sinus load at f_1 to develop the crack in B4 has caused bigger amplitude and thereby a higher stress level and extent of the yielding zone around the crack tip than in B3, B5 and B6, which were fatigued at f_2. The increases of ζ_1 for B5 and B6 are approximately twice the increases of ζ_1 for B3. This is probably due to that the curvature of the first mode shape is greater at $z = 0.1$ m (position of crack in B5 and B6) than at $z = 1.0$ m (position of crack in B3).
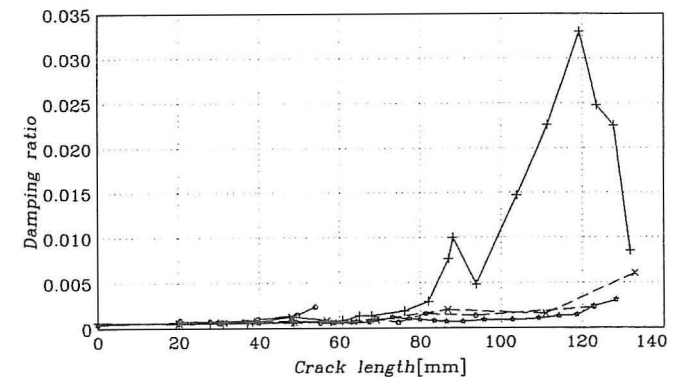
Figure 23 1st modal damping ratio

The variation of ζ_2 for B1-B3, B5 and B6 and ζ_3 for B5 is shown in figure 24 and figure 25 respectively. The estimated values are more scattered than the estimates for ζ_1 and it is impossible to recognize any trends. The scatter is caused by the same reasons mentioned above for ζ_1 combined with a lower signal to noise ratio.
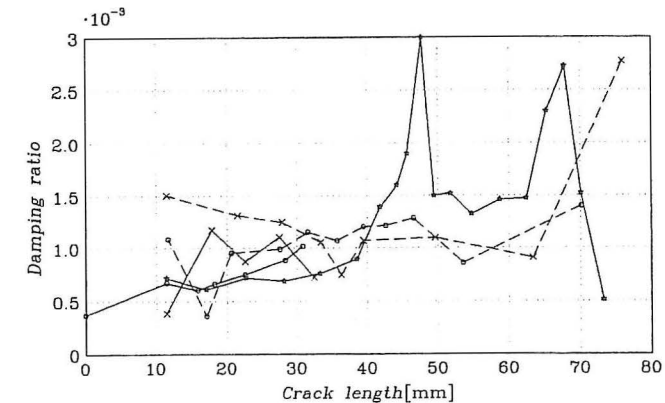
Figure 24 2nd modal damping ratio, beam B1-B3, B5 and B6.
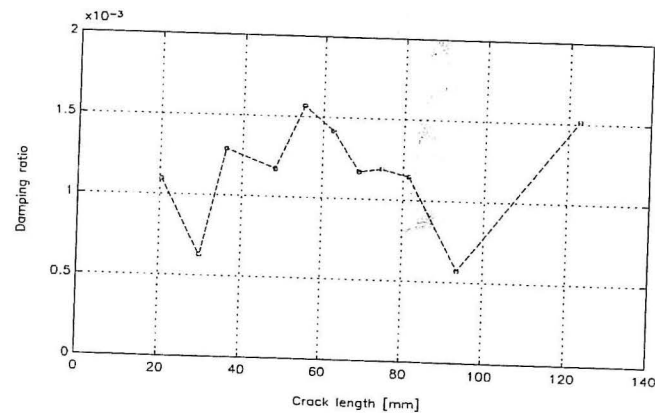
Figure 25 3rd modal damping ratio

4.3. MODE SHAPE RATIOS

The local bending stiffness of the beam at the crack will decrease towards zero as the crack grow. This means that the part of the beam, which is above the crack will move as a rigid body connected to the lower part by a hinge (see figure 26).
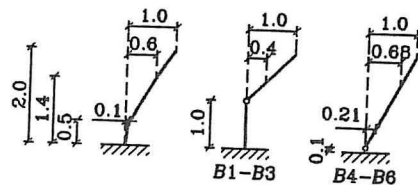
Figure 26 Deflection of beams, mode 1.

Figure 26 shows that Φ_{21}/Φ_{11} and Φ_{31}/Φ_{11} will respectively increase for B4-B6 and decrease for B1-B3. The mode shape values will move asymptotic against the values shown in figure 26 as a_{tot} grow. These tendencies are confirmed by the curves shown in figure 27 and figure 28.
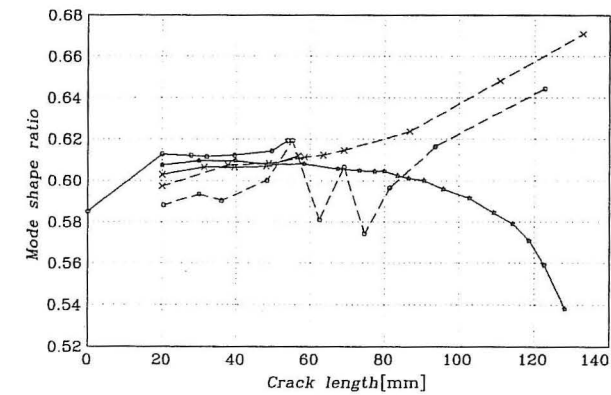
Figure 27 Mode no.1, mode shape ratio , Φ_{21}/Φ_{11}.
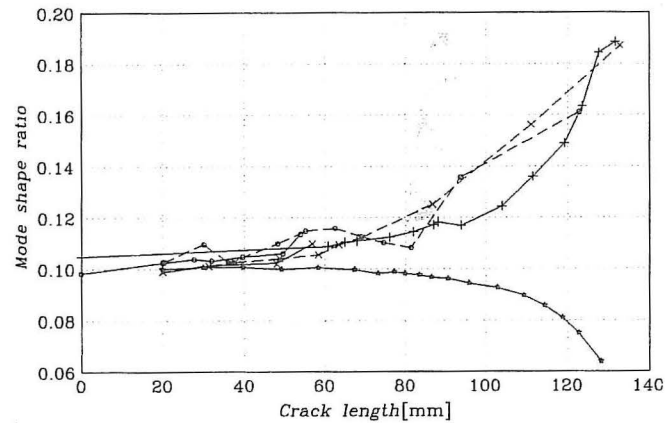
Figure 28 Mode no. 1, mode shape ratio , Φ_{31}/Φ_{11}.

Similar clear trends cannot be found the curves for Φ_{22}/Φ_{12} and Φ_{32}/Φ_{12} shown in figure 29 and figure 30. This agrees with the fact that the standard deviation on the estimates for mode shape ratios for mode 2 are considerable larger than the similar ratios for mode 1 (see e.g. table H1 in appendix H). The major reason for the pure results is that the estimations are based on measurements from free decays, where the first mode is dominant.
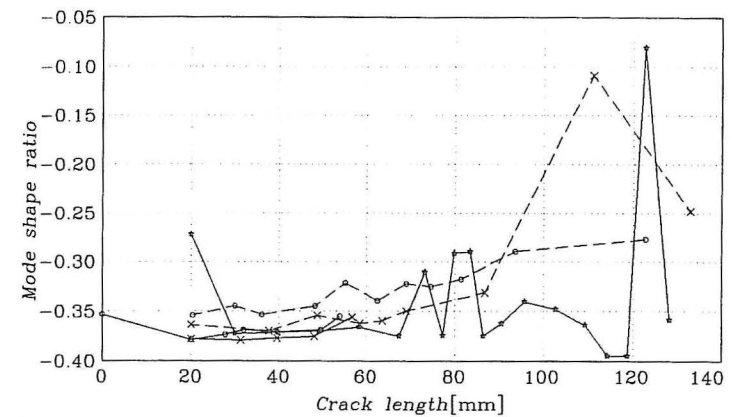
Figure 29 Mode no. 2, mode shape ratio , Φ_{22}/Φ_{12}.
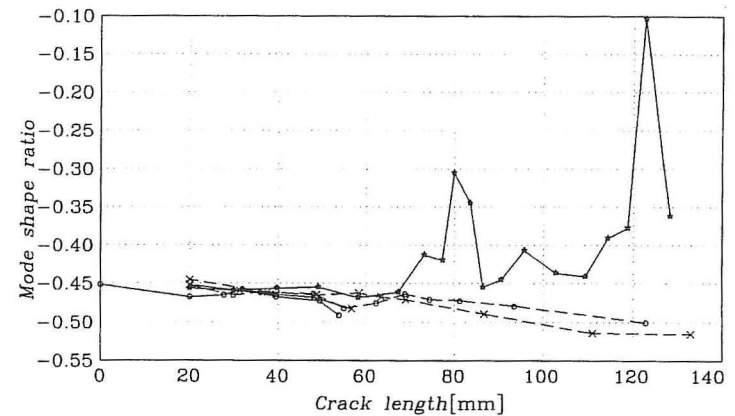
Figure 30 Mode no. 2, mode shape ratio , Φ_{32}/Φ_{12}.

5. DISCUSSION AND CONCLUSION

The results from the performed test series with six hollow sectioned steel cantilevers show that the modal parameters changes, when a fatigue crack is initiated and developed

in the beam.

Further it is observed that the beams becomes non-linear as the crack grow. However the degree of non-linearity depends on the amplitude of the vibrations. Therefore system identification methods developed for linear structures can also be used on cracked structures, as long as the amplitude of the vibrations is held under a certain level. Besides this phenomena is well known in connection with system identification of so-called linear structures.

The natural frequencies either decrease or remain unchanged, when the crack length is increased. The above mentioned amplitude depending non-linearity has only a negligible influence on the obtained estimates for the natural frequencies. The sensitivity of the single natural frequency depends on the location of the crack with respect to the curvature in the belonging mode shape. For instance f_3 for B3 remain almost constant for all crack length (see figure 20), while the other natural frequencies decrease. This is due to that the crack in B3 is placed in zero-point for the curvature of the third mode shape. However a non-changing modal parameter together with changing modal parameters will be of great importance in connection with a vibration based detection of the length and location of the crack. For example non-changing character of f_3 for B3 restrict from the beginning the possible area of damage to three local areas around the zero-points of the curvature of the third modes shape.

The modal damping ratio of the first mode increase by a factor of 2-70. However the estimates is highly depending on the amplitude level during the tests (see figure 23). The results indicates a relationship between the frequency of the sinus varying load used for fatigue and the increase in damping. Thus the use of modal damping ratios in connection with damage detection shall be performed with great care. The changes in the modal damping ratios shall primarily be used as qualitative damage indicators until the phenomenon has been investigated more detailed.

The results shows that mode shape ratios of the first mode moves asymptotic against boundary values corresponding to a rigid body movement of the beam section above the crack. Further it can be seen that influence on the mode shape ratios from above non-linearity seems to have minimal influence.

A common feature of the results is that the degree of uncertainty increase with the number of the mode. This is primarily due to that the system identification has been made from free decays, where the first mode is dominant. Thus the obtained curves for the modal parameters of mode 1 and the natural frequencies of mode 2-4 are quite

smooth. However skew crack growth has caused differences in the course of the curves for the single beams (see e.g. figure 18).

Another common feature is that the changes in the modal parameters are most pronounced for $a_{tot} > 80\,mm$. However the changes for $a_{tot} < 80\,mm$ are more interesting from damage detection point of view, because cracks with $a_{tot} > 80\,mm$ will probably be unacceptable. The tests have shown that the changes in the modal parameters are measurable for $a_{tot} < 80\,mm$. Therefore it is realistic to believe that the location and size of even small cracks ($a_{tot} < 60\,mm$) can be estimated from the measured parameters. This hope is confirmed by the results obtained in Rytter et al. [10], where the result from test G for B4 have been used a base for an evaluation of a damage diagnosing scheme (see table 1).

	Measured value	Estimated value
Crack position above the fixture, [mm]	100	100
Crack length, [mm]	61	64

Table 1 Results of vibration based diagnosing (Rytter et al [10]).

The tests have shown that different kinds of easy obtainable plots can be used to indicate damage (see figure 9 to figure 15).

It could be interesting to perform a new analog series of test to investigate the following topics

- loading frequency effect on damping
- other locations of cracks
- multiple crack situations
- use of other system identification methods for better estimates for higher modes
- the amplitude dependency of the damping

NOMENCLATURE

a_r : Length of right part of the crack

a_l : Length of left part of the crack

a_{tot} : Total length of crack $(a_{tot} = a_l + a_r)$

B1-B6   : Name of test beams

BW   : Band width in FRF [Hz]

$Cov(.)$: Covariance matrix

DOF   : Degree of freedom

E   : Modulus of elasticity

f_y : Yielding stress

f_{nd} : $n'th$ damped natural frequency [Hz]

f_n : $n'th$ natural frequency [Hz]

f_1^{virgin} : First natural frequency at the virgin state

$f_{i,x}$: $i'th$ natural frequency for vibration parallel to the x-axis

$f_{i,y}$: $i'th$ natural frequency for vibration parallel to the y-axis

f_s : Sampling frequency

$G_{x_i x_i}(f)$: Autospectral density function of the response in point i

$G_{F_j x_i}(f)$: Cross spectral density function between the load in point j and the response in point i

$H_{ij}(f)$: Frequency response function

I_y : Modulus of inertia with respect to the y-axis

i,j,k : index

N_p : Number of periods

P_θ : Asymptotic covariance matrix

$\hat{P}_N$: Estimate for P_θ

T_i^+ : Duration of the $i'th$ positive half-cycle

T_i^- : Duration of the $i'th$ negative half-cycle

t_i : Discrete time value

$V_N(\theta)$: Error function

X_i : Amplitude at the $i'th$ extreme

X_{ji} : Amplitude at measurement point j in mode i

x,y,z   : Cartesian coordinates

$x_i(t)$: Response at the $i'th$ measurement point.

$x^*(t_k)$: Filtered response

x_{zero} : DC-offset in signal if any

δ : Logarithmic decrement

ϵ : Prediction error

ζ_n : $n'th$ modal damping ratio

$\overline{\theta}$: System vector

λ_N : Variance

μ : Mass per length

σ : standard deviation

Φ_i : Modal coordinate at the $i'th$ measurement point of mode 1

Φ_i^+ : Φ_i for positive amplitudes

Φ_i^- : Φ_i for negative amplitudes

Φ_{ij} : Modal coordinate at point i of mode j

ϕ : Phase

ψ : Gradient of $\hat{x}(t_i|\overline{\theta})$ with respect to $\overline{\theta}$

$\hat{}$: Estimated parameter

REFERENCES

1. A. Rytter, *Vibration Based Inspection of Civil Engineering Structures* , Ph.D-thesis, University of Aalborg (to be published).

2. A. RYTTER, P. H. KIRKEGAARD and R. BRINCKER *An Experimental and Numerical study of the Modal Parameters of a Damaged Cantilever*, University of Aalborg (to be published).

3. D. WENDTLAND *Änderungen der Biegenfrequenzen einer idealisierten Schaufel durch Risse*, Ph.D-thesis, University of Karlsruhe, 1972.

4. F.D. JU AND M.E. MIMOVICH *Experimental Diagnosis of Fracture Damage in Structures by the Modal Frequency Method*, Journal of Vibration, Acoustics, Stress and Reliability in Design, Vol. 110, pp. 456-463, October 1988.

5. P. CAWLEY AND R. RAY *A Comparison of the Natural Frequency Changes Produced by Cracks and Slots* Journal of Vibration, Acoustics, Stress and Reliability in Design, Vol. 110, pp. 366-370, July 1988.

6. L. LJUNG *SYSTEM IDENTIFICATION, THEORY FOR THE USER*, Prentice Hall, 1987.

7. *OPTIMIZATION TOOLBOX, for use with MATLAB*, The Math Works, Inc., November, 1990.

8. STAR*Struct*-software , version 3.01, Structural Measurement Systems, 1989.

9. D. J. EWINS, *Modal Testing: Theory and Practice*, Research Studies Press LTD., 1985.

10. A. Rytter, R. Brincker and L. Pilegaard Hansen, *Detection of Fatigue Damage in a Steel Member,* Proceedings of the Florence Modal Analysis Conference, pp. 373-379,

APPENDIX A
Estimation of Covariance Matrix

The aim of this appendix is to investigate whether the asymptotic estimate for the covariance matrix given in equation (10)-(12) are applicable in connection with system identification based on curve fit of free decays. The expressions are tested for both a lightly damped system and normally damped system.

A.1. THE LIGHTLY DAMPED SYSTEM

The investigations are based on 1000 simulated of a ligthly damped system given by

$$x(t|\theta) = Xe^{-2\pi\zeta ft} \cos(\sqrt{1-\zeta^2}\, 2\pi ft + \phi) - x_{zero} + e(t) \qquad (A,1)$$

where

X : amplitude (= 1.0142)

ζ : damping ratio (= 0.482e-3)

f : frequency (= 11.3601 Hz)

ϕ : phase (= -0.5615 rad)

x_{zero} : displacement of the zeropoint (= -0.0005)

$e(t)$: Gaussian white noise with zero mean and variance $\sigma_e^2 = 0.23e{-3}$

The system parameters and the variance of the white noise have been taken from the fit on data from measurement point no. 1 serie B1_B1 (see appendix). Each simulation included 600 points with a sampling rate on 317.91 Hz ($\approx$ 28*f).

The system parameters were determined by minimizing the least square error function given in equation (8).

The asymptotic covariance matrix $Cov\hat{\theta}_{600}$ determined from data in the first of the simulations was

$$Cov\hat{\theta}_{600} = \begin{bmatrix} 3.12e{-}06 & 3.45e{-}08 & 2.81e{-}09 & -1.48e{-}08 & -1.22e{-}08 \\ x & 5.13e{-}10 & 4.38e{-}11 & -2.04e{-}10 & -6.97e{-}11 \\ x & x & 6.60e{-}08 & -3.79e{-}07 & 6.04e{-}10 \\ x & x & x & 2.95e{-}06 & -4.86e{-}09 \\ x & x & x & x & 3.73e{-}07 \end{bmatrix} \quad (A,2)$$

The sample covariance matrix for the 1000 curve fits was

$$Cov\hat{\theta}'_{1000} = \begin{bmatrix} 3.22e{-}06 & 3.55e{-}08 & 1.09e{-}08 & -1.66e{-}07 & -1.44e{-}08 \\ x & 5.28e{-}10 & 7.22e{-}11 & 1.55e{-}09 & 1.65e{-}10 \\ x & x & 6.54e{-}08 & -3.84e{-}07 & 9.29e{-}09 \\ x & x & x & 3.07e{-}06 & -9.29e{-}09 \\ x & x & x & x & 3.77e{-}07 \end{bmatrix} \quad (A,3)$$

The agreement between the diagonal elements of the two matrices is obvious.

A.2. THE NORMALLY DAMPED SYSTEM

The investigations are based on 1000 simulated of a ligthly damped system given by (A,1). In this case the following values of system parameters were used

X : amplitude (= 2.0798)

ζ : damping ratio (= 8.44e-3)

f : frequency (= 10.4431 Hz)

ϕ : phase (= 1.4325 rad)

x_{zero} : displacement of the zeropoint (= -0.0021)

$e(t)$: Gaussian white noise with zero mean and variance $\sigma_e^2 = 10.2e{-}3$

The system parameters and the variance of the white noise have been taken from the fit on data from measurement point no. 1 serie B4_L1 (see appendix). Each simulation included 600 points with a sampling rate on 317.91 Hz ($\approx$ 28*f).

The system parameters were determined by minimizing the least square error function given in equation (8).

The asymptotic covariance matrix $Cov\hat{\theta}_{600}$ determined from data in the first of the

simulations was

$$Cov\hat{\theta}_{600} = \begin{bmatrix} 2.73e{-}04 & 1.48e{-}06 & -3.01e{-}07 & 4.64e{-}06 & -1.40e{-}06 \\ x & 1.36e{-}08 & -6.34e{-}10 & 3.32e{-}08 & -7.84e{-}09 \\ x & x & 1.48e{-}06 & -7.60e{-}06 & -2.80e{-}07 \\ x & x & x & 6.68e{-}05 & -6.31e{-}07 \\ x & x & x & x & 1.65e{-}05 \end{bmatrix} \quad (A,4)$$

The sample covariance matrix for the 1000 curve fits was

$$Cov\hat{\theta}_{600} = \begin{bmatrix} 2.55e{-}04 & 1.35e{-}06 & -1.53e{-}07 & 2.20e{-}06 & -1.12e{-}07 \\ x & 1.26e{-}08 & -1.71e{-}09 & 1.82e{-}08 & 1.53e{-}09 \\ x & x & 1.39e{-}06 & -6.92e{-}06 & -6.26e{-}07 \\ x & x & x & 5.99e{-}05 & 5.79e{-}07 \\ x & x & x & x & 1.61e{-}05 \end{bmatrix} \quad (A,5)$$

The agreement between the diagonal elements of the two matrices is not so obvious as in the examle above. However the diagonal elements of the two matrices are of the same magnitude. Therefore in many cases it will be reasonable to use the expressions given by Ljung to get a rough estimates on the variances.

APPENDIX B
DIGITAL FILTERING OF FREE DECAYS

A digital lowpass and a digital bandpass elliptic filter have been used on the free decays before the performance of the curve fits (see figure B.1). The filter have been designed by mean of the Signal Processing Toolbox for use with MATLAB.

The frequency reponse of the digital elliptic filters of order n are given as
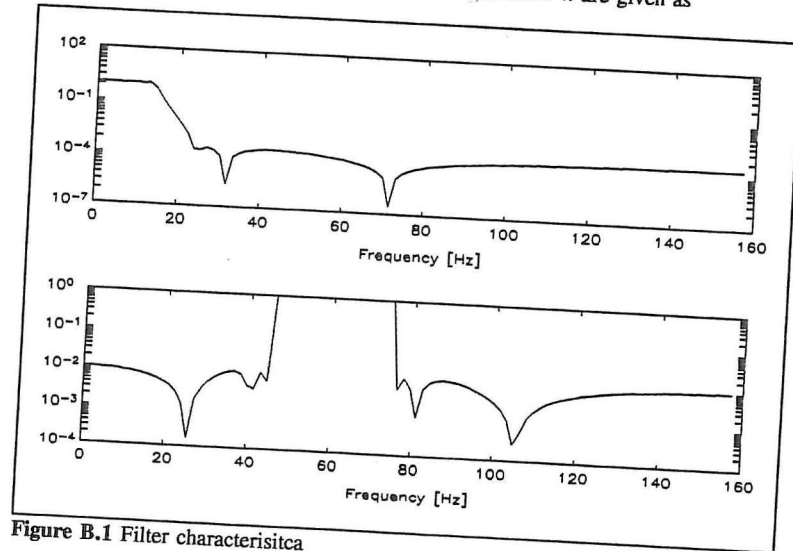
Figure B.1 Filter characterisitca

$$H(z) = \frac{\sum_{i=1}^{n+1} b_i z^{i-1}}{\sum_{i=1}^{n+1} a_i z^{i-1}}$$

The use of the digital filters causes a phase distortion and a distortion at the start of the signal due to the filter startup transients.

LOWPASS FILTER		
Filter order : 6 Cutoff frequency : 12.9 Hz Passband ripple : 0.1 dB Stopband attenuation : 72 dB		
i	a_i	b_i
1	1.000	0.405e-3
2	-5.4698	-1.498e-3
3	12.574	2.801e-3
4	-15.542	-3.356e-3
5	10.891	2.801e-3
6	-4.1010	-1.498e-3
7	0.6482	0.405e-3

Table B.1 Lowpass filter.

The phase distortion can be neglected as long as the same filter is used on all signals to be used together.

The noise on the free decays will be constant. This means that the signal to noise ratio will decrease as the amplitude decrease. Thus to obtain the best fit results one should use the first part of the free decay. Therefor the free decays have been filtered backwards. Thereby have the distortion due to the filter startup transients been "moved" from the start to the end of the signal (see figure B.2). The distort part of the signals have been excluded in the subsequent analysis.
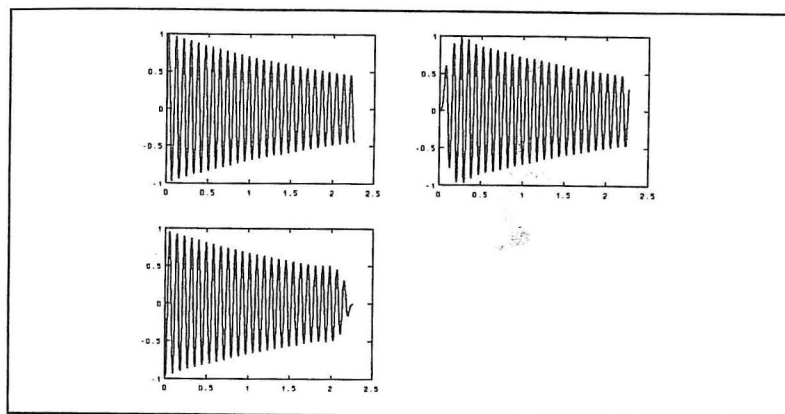
Figure B.2 Filtered signals

BANDPASS FILTER		
Filter order : 20 Cutoff freq., low: 45 Hz, high : 75 Hz Passband ripple : 0.1 dB Stopband attenuation : 72 dB		
i	ai	bi
1	1.000	0.014
2	-7.019	-0.092
3	30.223	0.358
4	-93.098	-1.012
5	228.022	2.299
6	-460.728	-4.375
7	792.827	7.202
8	-1178.660	-10.430
9	1534.066	13.484
10	-1757.422	-15.671
11	1781.414	16.474
12	-1597.558	-15.671
13	1267.463	13.484
14	-884.793	-10.430
15	540.490	7.202
16	-285.043	-4.375
17	127.932	2.299
18	-47.319	-1.012
19	13.907	0.358
20	-2.920	-0.092
21	0.377	0.014

Table B.2 Bandpass filter.

APPENDIX C
TEST RESULTS, Beam no. 1

Table C.1 Crack lengths

Test	Crack length		
	Left mm	Right mm	Total mm
A	0	0	0.00
B	10.00	10.00	20.00
C	13.87	13.81	27.68
D	16.00	15.96	31.96
E	19.69	19.86	39.55
F	24.87	24.70	49.57
G	26.96	26.96	53.92

Table C.2 Natural frequencies.

TEST	1st mode		2nd mode		3rd mode		4th mode	
	f Hz	σ_f Hz	f Hz	σ_f Hz	f Hz	BW Hz	f Hz	BW Hz
A	11.415	4.097e-5	71.103	1.309e-3	-	-	-	-
B	11.361	2.661e-5	70.832	6.889e-5	191.0	1	358	2
C	11.295	1.884e-5	70.352	5.183e-5	189.9	0.1	348	2
D	11.279	2.144e-5	70.208	6.516e-5	189.8	0.2	346	2
E	11.244	2.353e-5	69.921	6.543e-5	189.2	0.4	350	2
F	11.163	2.214e-5	69.388	6.460e-5	188.3	0.4	354	2
G	10.866	2.528e-5	68.031	8.867e-5	185.6	0.2	348	2

Table C.3 Natural frequencies. Lumped mass included.

TEST	1st mode		2nd mode		3rd mode		4th mode	
	f Hz	σ_f Hz	f Hz	σ_f Hz	f Hz	BW Hz	f Hz	BW Hz
B_m1	10.782	2.5e-5	70.485	7.2e-5	190	1	352	2
B_m2	11.326	2.6e-5	68.448	7.1e-5	184.5	0.1	357	2

Table C.4 Modal damping ratios.

TEST	1st mode		2nd mode	
	ς	σ_ς	ς	σ_ς
A	4.377e-04	3.594e-06	3.699e-04	1.840e-05
B	6.245e-04	2.349e-06	6.733e-04	9.729e-07
C	7.479e-04	1.655e-06	6.033e-04	7.365e-07
D	7.089e-04	1.897e-06	6.627e-04	9.276e-07
E	9.671e-04	2.105e-06	7.486e-04	9.351e-07
F	1.459e-03	1.985e-06	8.843e-04	9.307e-07
G	2.351e-03	2.336e-06	1.018e-03	1.303e-06

Table C.5 Modal damping ratios. Lumped mass included.

TEST	1st mode		2nd mode	
	ς	σ_ς	ς	σ_ς
B_m1	6.390e-04	6.440e-04	6.314e-04	6.408e-04
B_m2	7.029e-04	7.009e-04	6.827e-04	7.007e-04

A. RYTTER ET AL.

Table C.6 Mode shape ratios.

TEST	1st mode				2nd mode			
	ϕ_2/ϕ_1		ϕ_3/ϕ_1		ϕ_2/ϕ_1		ϕ_3/ϕ_1	
	Est	σ	Est.	σ	Est.	σ	Est.	σ
A	0.585	4.133e-4	0.098	1.732e-4	-0.353	9.476e-3	-0.452	9.967e-4
B	0.613	2.340e-4	0.102	6.991e-5	-0.379	5.148e-4	-0.468	4.95e-4
C	0.612	1.594e-4	0.104	5.577e-5	-0.374	3.951e-4	-0.465	3.53e-4
D	0.612	1.850e-4	0.103	7.175e-5	-0.369	5.040e-4	-0.458	4.73e-4
E	0.612	2.060e-4	0.105	6.509e-5	-0.371	4.696e-4	-0.468	4.25e-4
F	0.614	2.238e-4	0.106	6.294e-5	-0.369	4.282e-4	-0.472	4.12e-4
G	0.619	2.184e-4	0.113	7.416e-5	-0.355	5.238e-4	-0.491	6.25e-4

Table C.7 Mode shape ratios. Lumped mass included.

TEST	1st mode				2nd mode			
	ϕ_2/ϕ_1		ϕ_3/ϕ_1		ϕ_2/ϕ_1		ϕ_3/ϕ_1	
	Est.	σ	Est.	σ	Est.	σ	Est.	σ
B_m1	0.613	2.156e-4	0.101	8.460e-5	-0.416	6.566e-4	-0.487	4.996e-4
B_m2	0.617	2.246e-4	0.102	7.150e-5	-0.354	5.894e-4	-0.464	4.380e-4

Table D.1 Crack lengths

Test	Crack length		
	Left mm	Right mm	Total mm
A	0	0	0.00
B	10.00	10.00	20.00
C	13.87	13.81	27.68
D	16.00	15.96	31.96
E	19.69	19.86	39.55
F	Fatigue crack developed at the fixture		

Table D.2 Natural frequencies.

TEST	1st mode		2nd mode		3rd mode		4th mode	
	f Hz	σ_f Hz	f Hz	σ_f Hz	f Hz	BW Hz	f Hz	BW Hz
A	11.460	9.860e-5	70.754[1]	0.146[2]	187.9[1]	0.39	-	-
B	11.447	2.142e-5	71.189	5.119e-5	191.7	0.1	357	2
C	11.379	2.013e-5	70.656	6.853e-5	190.9	0.1	354	2
D	11.355	1.822e-5	70.355	6.882e-5	190.6	0.1	350	2
E	11.332	1.770e-5	70.041	5.704e-5	190.5	0.1	352	2
F	10.960	1.614e-5	67.861	4.645e-5	186.3	0.1	346	2

1) White noise load attached by mean of a shaker
2) Bandwidth

Table D.3 Modal damping ratios.

TEST	1st mode		2nd mode	
	ζ	σ_ζ	ζ	σ_ζ
A	1.66e-03[1]	8.451e-06		
B	6.245e-04	2.349e-06	6.733e-04	9.729e-07
C	7.479e-04	1.655e-06	6.033e-04	7.365e-07
D	7.089e-04	1.897e-06	6.627e-04	9.276e-07
E	9.671e-04	2.105e-06	7.486e-04	9.351e-07
F	1.459e-03	1.985e-06	8.843e-04	9.307e-07

1) Shaker mounted during the free decay tests.

Table D.4 Mode shape ratios.

TEST	1st mode				2nd mode			
	$\hat{\xi}_2/\hat{\xi}_1$		$\hat{\xi}_3/\hat{\xi}_1$		$\hat{\xi}_2/\hat{\xi}_1$		$\hat{\xi}_3/\hat{\xi}_1$	
	Est	σ	Est.	σ	Est.	σ	Est.	σ
A	0.585	9.607e-4	0.091	-	-	-	-	-
B	0.603	1.821e-4	0.099	6.056e-5	-0.378	3.467e-4	-0.452	3.916e-4
C	0.607	1.710e-4	0.101	5.528e-5	-0.379	6.095e-4	-0.460	4.121e-4
D	0.607	1.542e-4	0.102	4.572e-5	-0.377	5.711e-4	-0.465	4.784e-4
E	0.607	1.482e-4	0.102	4.373e-5	-0.375	4.147e-4	-0.468	3.454e-4
F	0.612	1.361e-4	0.110	4.531e-5	-0.356	3.740e-4	-0.483	3.286e-4

APPENDIX E
TEST RESULTS, Beam no. 3

Table E.1 Crack lengths

Test	Crack length		
	Left mm	Right mm	Total mm
A	0	0	0.00
B	10.00	10.00	20.00
C	14.88	15.02	29.90
D	19.57	20.19	39.76
E	24.01	25.24	49.25
F	28.15	30.18	58.33
G	32.31	35.10	67.41
H	35.19	37.86	73.05
I	36.92	39.00	75.92
J	38.91	40.96	79.87
K	40.40	43.08	83.48
L	41.88	44.58	86.47
M	43.68	46.88	90.57
N	46.58	49.18	95.77
O	50.78	51.98	102.77
P	54.38	54.88	109.27
Q	57.08	57.18	114.27
R	58.98	59.68	118.67
S	60.88	61.78	122.67
T	63.78	64.38	128.17
U	65.88	66.38	132.27
V	83.00	83.00	166.00

Table E.2 Natural frequencies.

TEST	1st mode		2nd mode		3rd mode		4th mode	
	f Hz	σ_f Hz	f Hz	σ_f Hz	f Hz	BW Hz	f Hz	BW Hz
A	11.351	03.04e-05	70.94	0.04*	190.7	0.1	. -	-
B	11.418	2.502e-05	71.123	1.122e-04	191.6	0.1	356	2
C	11.389	1.710e-05	70.874	4.383e-05	191.5	0.1	358	2
D	11.378	1.678e-05	70.636	5.490e-05	191.2	0.1	354	2
E	11.36	1.689e-05	70.284	5.453e-05	191.1	0.1	350	2
F	11.338	1.792e-05	69.730	8.197e-05	191.4	0.1	350	2
G	11.308	1.688e-05	69.017	7.977e-05	191.2	0.1	350	2
H	11.289	1.703e-05	68.603	2.971e-04	191.1	0.1	348	2
I	11.268	1.754e-05	68.099	5.450e-04	191.1	0.1	346	2
J	11.26	1.877e-05	67.909	5.909e-04	191.1	0.1	344	2
K	11.239	1.776e-05	67.401	7.121e-04	191.1	0.1	342	2
L	11.204	1.885e-05	66.705	2.144e-04	191.1	0.1	338	2
M	11.172	1.882e-05	66.123	1.384e-04	191	0.1	340	2
N	11.108	1.981e-05	64.848	1.708e-04	191.1	0.1	334	2
O	11.006	1.977e-05	62.849	1.265e-04	191.3	0.1	330	2
P	10.863	1.834e-05	60.558	1.336e-04	191.2	0.1	322	2
Q	10.698	1.661e-05	58.291	3.993e-04	191.3	0.1	316	2
R	10.496	1.611e-05	55.876	6.313e-04	191.1	0.1	310	2
S	10.183	1.639e-05	51.267	2.129e-03	191	0.1	300	2
T	9.5623	3.653e-05	47.725	8.101e-04	191.1	0.1	292	2
U	8.85	0.04*	43.80	0.2*	191	0.1	282	2
V	3.2	0.04*	33.20	0.2*	189	0.1	254	2

* : Bandwidth, [Hz].

Table E.3 Modal damping ratios.

TEST	1st mode		2nd mode	
	ξ	σ_ξ	ξ	σ_ξ
A	4.2e-04	2.68e-06	-	-
B	7.111e-04	2.189e-06	7.181e-04	1.576e-06
C	7.402e-04	1.501e-06	6.100e-04	6.182e-07
D	5.652e-04	1.477e-06	7.191e-04	7.776e-07
E	7.179e-04	1.493e-06	6.873e-04	7.764e-07
F	5.512e-04	1.578e-06	7.582e-04	1.178e-06
G	6.457e-04	1.503e-06	8.920e-04	1.156e-06
H	1.177e-03	1.486e-06	1.387e-03	4.337e-06
I	1.026e-03	1.567e-06	1.600e-03	8.020e-06
J	9.470e-04	1.672e-06	1.900e-03	8.707e-06
K	7.643e-04	1.588e-06	2.996e-03	1.059e-05
L	6.834e-04	1.676e-06	1.498e-03	3.212e-06
M	6.877e-04	1.677e-06	1.518e-03	2.096e-06
N	8.745e-04	1.782e-06	1.318e-03	2.632e-06
O	8.696e-04	1.784e-06	1.457e-03	2.012e-06
P	1.035e-03	1.687e-06	1.471e-03	2.203e-06
Q	1.293e-03	1.563e-06	2.301e-03	6.850e-06
R	1.398e-03	1.530e-06	2.723e-03	1.130e-05
S	2.365e-03	1.613e-06	1.522e-03	4.158e-05
T	3.076e-03	3.823e-06	5.082e-04	1.697e-05

A. RYTTER ET AL.

Table E.4 Mode shape ratios.

TEST	1st mode				2nd mode			
	$\tilde{e}_2/\tilde{e}_1$		$\tilde{e}_3/\tilde{e}_1$		$\tilde{e}_2/\tilde{e}_1$		$\tilde{e}_3/\tilde{e}_1$	
	Est.	σ	Est.	σ	Est.	σ	Est.	σ
A	0.586	1.53e-04	0.100	-	-	-	-	-
B	0.607	2.271e-04	0.100	6.665e-05	-0.273	1.114e-03	-0.457	7.077e-04
C	0.609	1.555e-04	0.101	3.280e-05	-0.372	3.336e-04	-0.459	2.869e-04
D	0.610	1.542e-04	0.101	3.125e-05	-0.371	5.228e-04	-0.457	3.888e-04
E	0.608	1.510e-04	0.100	3.346e-05	-0.370	4.740e-04	-0.455	3.630e-04
F	0.608	1.676e-04	0.100	3.605e-05	-0.366	5.657e-04	-0.469	6.650e-04
G	0.606	1.492e-04	0.100	3.471e-05	-0.375	6.502e-04	-0.461	5.164e-04
H	0.605	1.437e-04	0.098	3.378e-05	-0.311	1.725e-03	-0.413	1.648e-03
I	0.604	1.538e-04	0.099	3.466e-05	-0.375	2.784e-03	-0.420	3.264e-03
J	0.605	1.604e-04	0.098	4.230e-05	-0.291	3.306e-03	-0.305	3.800e-03
K	0.602	1.561e-04	0.098	3.466e-05	-0.290	2.301e-03	-0.345	2.433e-03
L	0.601	1.621e-04	0.097	4.725e-05	-0.375	1.142e-03	-0.455	1.137e-03
M	0.600	1.591e-04	0.096	5.161e-05	-0.362	8.993e-04	-0.445	7.851e-04
N	0.596	1.619e-04	0.094	5.653e-05	-0.340	9.374e-04	-0.407	1.424e-03
O	0.591	1.565e-04	0.093	8.270e-05	-0.348	7.420e-04	-0.436	8.303e-04
P	0.585	1.433e-04	0.090	7.393e-05	-0.364	7.616e-04	-0.441	7.532e-04
Q	0.579	1.303e-04	0.086	4.924e-05	-0.395	1.718e-03	-0.391	2.084e-03
R	0.571	1.226e-04	0.081	5.679e-05	-0.395	2.655e-03	-0.377	2.733e-03
S	0.559	1.197e-04	0.075	6.106e-05	-0.080	1.085e-02	-0.104	1.269e-02
T	0.538	2.559e-04	0.064	8.415e-05	-0.358	6.181e-03	-0.362	6.028e-03

APPENDIX F
TEST RESULTS, Beam no. 4

Table F.1 Crack lengths

Test	Crack length		
	Left mm	Right mm	Total mm
A	0.0	0.0	0.0
B	10.0	10.0	20.0
C	14.0	13.7	27.7
D	15.0	16.0	31.0
E	18.5	18.5	37.0
F	24.0	24.6	48.6
G	30.4	30.4	60.8
H	33.0	32.0	65.0
I	34.6	33.4	68.0
J	40.5	35.5	76.0
K	43.0	39.0	82.0
L	44.0	43.0	87.0
M	44.7	43.4	88.1
N	47.4	46.4	93.8
O	51.5	52.4	103.9
P	57.2	54.2	111.4
Q	58.3	60.9	119.2
R	60.1	63.4	123.5
S	61.5	66.1	127.6

The instrumentation has due to inexplicable reasons been changed during test B-E. One accelerometer at the top and at the middle of the beam were used during these tests.

Table F.2 Natural frequencies.

TEST	1st mode		2nd mode		3rd mode	
	f Hz	σ_f Hz	f Hz	BW Hz	f Hz	BW Hz
A	11.309	2.418e-03	70.48	0.02	190	2
B	11.227	1.408e-02				
C	11.191	6.149e-03				
D	11.182	1.951e-04				
E	11.164	1.360e-03				
F	11.09	2.113e-03	69.40	0.02		
G	10.923	1.845e-03	69.12	0.02		
H	10.866	1.496e-03	67.86	0.02	187.1	0.1
I	10.847	2.358e-03	67.79	0.02		
J	10.672	1.088e-03	68.36	0.02	186.4	0.1
K	10.542	4.825e-03	68.00			
L	10.413	1.684e-02				
M	10.379	1.871e-02				
N	10.427	4.743e-03				
O	10.041	6.472e-02				
P	9.2659	1.793e-02				
Q	8.1932	2.016e-02				
R	7.2021	4.404e-02	61.6	0.4	178.8	0.4
S	6.0278	1.092e-01	59.6	0.4	177.0	0.4

Table F.3 Modal damping ratios.

TEST	1st mode	
	ξ	σ_ξ
A	6.044e-04	7.861e-05
B	4.794e-04	4.500e-05
C	5.370e-04	2.268e-05
D	5.312e-04	9.019e-06
E	5.036e-04	2.669e-05
F	6.913e-04	5.278e-05
G	8.256e-04	7.422e-05
H	1.346e-03	9.067e-05
I	1.363e-03	1.027e-04
J	1.854e-03	2.860e-05
K	2.950e-03	2.182e-04
L	7.654e-03	5.994e-04
M	9.974e-03	4.759e-04
N	4.815e-03	3.212e-04
O	1.469e-02	7.846e-04
P	2.257e-02	2.099e-03
Q	3.295e-02	4.470e-03
R	2.475e-02	4.072e-03
S	2.250e-02	5.190e-03

A. RYTTER ET AL.

Table F.4 Mode shape ratios.

TEST	1st mode			
	ξ_3/ξ_1		ξ_4/ξ_1	
	Est.	σ	Est.	σ
A	0.10467	2.257e-05		
B			0.35316	7.109e-04
C			0.34254	1.174e-03
D			0.34298	1.724e-04
E			0.34452	3.444e-04
F	0.10467	1.682e-04		
G	0.10866	1.208e-04		
H	0.11036	1.153e-04		
I	0.11076	1.530e-04		
J	0.11225	9.312e-05		
K	0.11433	1.285e-04		
L	0.11718	1.682e-04		
M	0.11823	3.802e-04		
N	0.1169	1.368e-04		
O	0.12448	6.477e-04		
P	0.13593	1.676e-03		
Q	0.14899	1.696e-03		
R	0.16343	7.320e-04		
S	0.1842	8.671e-03		

APPENDIX G
TEST RESULTS, Beam no. 5

Table G.1 Crack lengths

Test	Crack length		
	Left mm	Right mm	Total mm
A	0	0	0.00
B	9.90	10.50	20.40
C	14.80	15.20	30.00
D	17.80	18.30	36.10
E	23.20	25.10	48.30
F	25.80	29.40	55.20
G	28.30	34.20	62.50
H	30.10	39.00	69.10
I	31.30	43.28	74.58
J	32.40	48.98	81.38
K	34.40	59.28	93.68
L	47.58	75.18	122.77

Table G.2 Natural frequencies.

TEST	1st mode f Hz	2nd mode f Hz	3rd mode f Hz
A	11.368[1)	70.9[2)	. . . . 190.4[3)
B	11.460	71.333	191.782
C	11.409	71.096	191.177
D	11.370	70.893	190.894
E	11.270	70.541	190.413
F	11.161	70.191	190.032
G	11.070	69.858	189.512
H	10.858	69.141	188.349
I	10.732	68.772	187.850
J	10.334	67.672	186.664
K	9.453	65.750	184.409
L	7.615	63.031	181.721

1) Curve fit
2) BW = 0.1 Hz
3) BW = 0.2 Hz

Table G.3 Modal damping ratios.

TEST	1st mode ζ o/oo	2nd mode ζ o/oo	3rd mode ζ o/oo
A	0.7182	-	-
B	0.8543	1.0860	1.0940
C	0.5701	0.3606	0.6283
D	0.7744	0.9540	1.2870
E	0.7960	0.9899	1.1720
F	0.5802	1.1510	1.5680
G	0.7657	1.0680	1.4160
H	1.0040	1.2010	1.1680
I	0.6210	1.2120	1.1890
J	1.5780	1.2810	1.1440
K	1.3570	0.8559	0.5718
L	2.2800	1.3990	1.5130

The Fit Errors shown in the following tables range from between 0 and 100, with values close to 0 being good and numbers approaching 100 are bad (see [8]).

Table G.4 Mode shapes, test B.

Point no.	1st mode			2nd mode			3rd mode		
	$|\phi_{1i}|$	Phase Deg.	Error	$|\phi_{2i}|$	Phase Deg.	Error	$|\phi_{3i}|$	Phase Deg	Error
1	serie C	179.54	3.22	109.13	-1.64	0.0468	457.21	178.24	0.163
2	4.120	179.75	3.18	83.00	-1.27	0.0436	280.07	178.62	0.157
3	3.800	-179.53	3.12	56.09	-1.76	0.0380	89.52	178.50	0.134
4	3.490	-179.62	3.08	30.35	-1.34	0.0238	85.00	-1.01	0.201
5	3.190	-179.66	3.04	5.20	-1.56	0.0506	221.40	-1.66	0.177
6	2.900	-179.78	2.95	17.44	179.28	0.1292	309.83	-1.42	0.169
7	2.590	-179.81	2.87	37.60	178.33	0.0821	342.74	-1.30	0.162
8	2.300	179.47	2.87	54.88	178.50	0.0679	320.41	-0.98	0.153
9	2.040	178.87	2.73	68.03	178.49	0.0607	240.04	-1.21	0.140
10	1.830	179.71	2.60	77.81	178.49	0.0550	127.36	-1.16	0.104
11	1.470	177.82	2.58	82.64	178.43	0.0496	11.44	173.87	1.670
12	1.310	-179.76	2.45	83.20	178.43	0.0448	154.70	177.78	0.237
13	1.030	-179.73	2.34	79.58	178.37	0.0396	272.33	178.25	0.204
14	0.842	178.37	2.18	73.06	178.41	0.0347	360.88	178.89	0.191
15	0.646	178.52	2.06	62.86	178.53	0.0299	404.82	179.05	0.182
16	0.479	175.89	1.78	50.78	178.43	0.0277	393.69	178.60	0.182
17	0.301	173.18	1.90	37.11	178.44	0.0218	335.17	176.83	0.171
18	0.196	173.06	2.42	24.66	178.48	0.0198	246.25	176.87	0.167
19	0.128	148.52	3.98	13.73	178.30	0.0182	153.39	177.49	0.166
20	0.065	157.30	5.05	4.18	178.42	0.0158	53.88	-179.14	0.182

Table G.5 Mode shapes, test C.

Point no.	1st mode			2nd mode			3rd mode		
	$|\phi_{1i}|$	Phase Deg.	Error	$|\phi_{2i}|$	Phase Deg.	Error	$|\phi_{3i}|$	Phase Deg	Error
1	4.370	179.54	3.22	109.13	-1.64	0.0468	457.21	178.24	0.163
2	4.120	179.75	3.18	83.00	-1.27	0.0436	280.07	178.62	0.157
3	3.800	-179.53	3.12	56.09	-1.76	0.0380	89.52	178.50	0.134
4	3.490	-179.62	3.08	30.35	-1.34	0.0238	85.00	-1.01	0.201
5	3.190	-179.66	3.04	5.20	-1.56	0.0506	221.40	-1.66	0.177
6	2.900	-179.78	2.95	17.44	179.28	0.1292	309.83	-1.42	0.169
7	2.590	-179.81	2.87	37.60	178.33	0.0821	342.74	-1.30	0.162
8	2.300	179.47	2.87	54.88	178.50	0.0679	320.41	-0.98	0.153
9	2.040	178.87	2.73	68.03	178.49	0.0607	240.04	-1.21	0.140
10	1.830	179.71	2.60	77.81	178.49	0.0550	127.36	-1.16	0.104
11	1.470	177.82	2.58	82.64	178.43	0.0496	11.44	173.87	1.670
12	1.310	-179.76	2.45	83.20	178.43	0.0448	154.70	177.78	0.237
13	1.030	-179.73	2.34	79.58	178.37	0.0396	272.33	178.25	0.204
14	0.842	178.37	2.18	73.06	178.41	0.0347	360.88	178.89	0.191
15	0.646	178.52	2.06	62.86	178.53	0.0299	404.82	179.05	0.182
16	0.479	175.89	1.78	50.78	178.43	0.0277	393.69	178.60	0.182
17	0.301	173.18	1.90	37.11	178.44	0.0218	335.17	176.83	0.171
18	0.196	173.06	2.42	24.66	178.48	0.0198	246.25	176.87	0.167
19	0.128	148.52	3.98	13.73	178.30	0.0182	153.39	177.49	0.166
20	0.065	157.30	5.05	4.18	178.42	0.0158	53.88	-179.14	0.182

Table G.6 Mode shapes, test D.

Point no.	1st mode			2nd mode			3rd mode		
	$\|\Phi_{1i}\|$	Phase Deg.	Error	$\|\Phi_{2i}\|$	Phase Deg.	Error	$\|\Phi_{3i}\|$	Phase Deg	Error
1	4.40	-179.74	3.22	108.90	-0.135	0.0512	455.79	179.87	0.195
2	4.06	-179.99	3.19	83.52	-0.105	0.0508	277.16	179.82	0.196
3	3.78	-178.27	3.15	56.57	0.282	0.0460	85.88	-179.98	0.167
4	3.52	180.00	3.10	29.87	0.486	0.0301	88.08	-0.41	0.266
5	3.25	-178.96	3.04	5.18	0.705	0.0711	225.78	-0.68	0.230
6	2.93	179.67	2.98	17.51	-179.59	0.1635	313.08	-0.78	0.215
7	2.60	-179.02	2.94	38.49	-179.54	0.1004	343.33	-0.37	0.205
8	2.32	179.94	2.85	56.63	-179.75	0.0823	322.41	-0.38	0.192
9	2.07	-179.88	2.77	69.40	179.98	0.0717	249.51	-0.01	0.176
10	1.79	179.89	2.65	78.22	179.68	0.0636	131.31	0.01	0.132
11	1.51	179.04	2.50	83.26	179.58	0.0572	12.05	174.39	1.920
12	1.28	179.18	2.35	83.74	179.58	0.0518	150.68	179.34	0.307
13	1.07	179.38	2.19	80.55	179.67	0.0467	270.67	179.41	0.255
14	0.853	177.95	1.99	73.63	179.65	0.0415	360.99	179.52	0.233
15	0.648	178.42	1.79	63.67	179.80	0.0381	404.17	179.74	0.222
16	0.450	174.18	1.61	50.29	179.83	0.0389	391.51	179.78	0.218
17	.0.293	176.12	1.52	37.89	179.85	0.0335	341.96	179.76	0.207
18	0.199	167.39	1.56	25.71	-179.92	0.0322	258.19	179.81	0.203
19	0.127	161.12	1.92	14.31	-179.55	0.0385	155.76	179.63	0.208
20	0.135	-179.19	2.44	4.92	-178.99	0.0437	62.53	178.88	0.217

Table G.7 Mode shapes, test E.

Point no.	1st mode			2nd mode			3rd mode		
	$\|\Phi_{1i}\|$	Phase Deg.	Error	$\|\Phi_{2i}\|$	Phase Deg.	Error e-3	$\|\Phi_{3i}\|$	Phase Deg	Error e-3
1	4.54	-177.93	3.02	108.91	-0.39	52.92	458.44	-179.65	170.71
2	4.15	-179.83	2.98	83.53	-0.41	49.63	280.29	-179.71	167.78
3	3.88	179.51	2.99	56.21	-0.22	44.82	87.40	-179.81	141.50
4	3.64	179.40	2.92	30.57	0.84	30.26	85.20	0.73	228.60
5	3.41	177.77	2.81	6.04	0.58	49.31	223.55	0.15	197.04
6	2.99	179.04	2.79	17.43	179.56	158.22	314.17	-0.08	182.95
7	2.72	178.70	2.64	37.53	-179.38	97.24	345.29	-0.16	174.4
8	2.40	179.31	2.59	55.11	179.48	77.81	323.33	-0.02	163.97
9	2.12	179.33	2.59	67.77	179.24	68.07	250.95	0.04	147.87
10	1.81	179.57	2.48	77.44	179.24	59.73	130.20	-0.10	106.28
11	1.60	178.46	2.37	82.32	179.09	53.93	4.85	165.90	3.19e3
12	1.33	178.88	2.21	82.87	179.08	48.51	143.59	179.14	269.49
13	1.09	178.22	1.98	79.82	179.27	42.54	271.44	179.55	214.02
14	0.875	178.76	1.90	73.13	178.9	37.59	355.65	179.50	195.40
15	0.680	177.51	1.60	63.27	179.12	32.92	400.20	179.65	184.38
16	0.498	178.65	1.55	50.47	179.06	32.03	391.14	179.41	183.04
17	0.323	173.74	1.57	37.89	178.93	27.29	340.65	179.44	173.96
18	0.222	172.53	2.08	26.30	179	26.45	262.37	179.68	171.12
19	0.094	161.22	4.83	14.48	179.28	29.75	160.76	179.72	171.64
20	0.061	119.74	7.84	5.75	-179.79	41.48	72.42	179.35	179.90

Table G.8 Mode shapes, test F.

Point no.	1st mode			2nd mode			3rd mode		
	$|\phi_{1i}|$	Phase Deg.	Error	$|\phi_{2i}|$	Phase Deg.	Error	$|\phi_{3i}|$	Phase Deg	Error
1	4.36	178.66	3.00	111.30	-0.506	0.0551	459.24	179.79	0.188
2	4.16	179.51	2.86	85.20	-0.504	0.0523	280.59	179.94	0.186
3	3.82	179.89	2.85	57.70	-0.229	0.0470	89.01	-179.74	0.160
4	3.58	-179.22	2.80	31.62	0.650	0.0377	84.83	0.39	0.257
5	3.36	-178.36	2.71	6.35	0.085	0.0553	218.45	0.04	0.215
6	3.03	176.97	2.72	17.18	-179.64	0.1808	307.5	-0.33	0.204
7	2.70	179.25	2.60	35.79	-179.95	0.1101	342.56	0.04	0.190
8	2.37	177.69	2.62	55.36	179.43	0.0836	326	0.02	0.175
9	2.13	-179.83	2.52	68.90	179.20	0.0711	253.13	0.00	0.158
10	1.82	179.59	2.47	78.61	179.12	0.0615	134.54	0.04	0.118
11	1.57	179.62	2.34	83.43	179.11	0.0553	5.13	162.85	3.510
12	1.26	176.82	2.31	84.35	179.05	0.0490	147.49	178.70	0.303
13	1.06	178.57	2.13	80.60	178.90	0.0446	268.25	179.53	0.235
14	0.844	179.45	1.99	74.19	178.57	0.0405	356.16	179.54	0.209
15	0.669	177.53	1.71	64.53	178.87	0.0380	402.24	179.41	0.196
16	0.501	179.16	1.59	53.63	179.12	0.0391	395.08	179.72	0.196
17	0.318	175.61	1.55	38.86	179.09	0.0369	340.17	179.45	0.184
18	0.218	172.21	1.51	25.73	179.17	0.0351	252.20	179.31	0.185
19	0.145	164.46	1.18	14.50	178.64	0.0349	155.25	179.24	0.191
20	0.021	151.82	12.40	5.32	178.48	0.0549	65.07	177.79	0.216

Table G.9 Mode shapes, test G.

Point no.	1st mode			2nd mode			3rd mode		
	$|\phi_{1i}|$	Phase Deg.	Error	$|\phi_{2i}|$	Phase Deg.	Error	$|\phi_{3i}|$	Phase Deg	Error
1	4.43	178.99	2.59	109.16	1.68	0.055	454.65	-179.72	0.155
2	4.11	179.32	2.46	84.08	-0.25	0.052	278.81	179.99	0.147
3	3.86	178.89	2.42	57.32	0.66	0.046	88.18	-179.76	0.125
4	3.56	177.72	2.38	30.91	0.71	0.031	85.57	0.18	0.209
5	3.30	178.74	2.30	5.82	0.96	0.060	220.90	-0.67	0.178
6	2.91	177.17	2.25	16.61	-179.98	0.156	305.78	-0.86	0.167
7	2.57	179.11	2.19	37.04	-179.91	0.093	338.86	-0.51	0.154
8	2.31	177.42	2.07	54.16	-179.33	0.076	320.03	0.24	0.144
9	2.05	178.06	1.98	66.83	-179.77	0.068	251.43	0.25	0.130
10	1.81	175.58	1.92	78.16	179.84	0.061	133.37	0.15	0.091
11	1.58	175.88	1.84	83.14	-179.99	0.054	2.67	46.64	3.340
12	1.33	177.98	1.71	84.00	179.87	0.049	141.36	179.16	0.250
13	1.09	177.03	1.59	80.80	179.81	0.043	262.66	179.28	0.194
14	0.856	177.43	1.48	74.33	179.66	0.039	352.66	179.35	0.175
15	0.672	174.42	1.34	64.68	179.84	0.035	396.06	179.65	0.164
16	0.512	173.04	1.36	51.87	179.87	0.033	387.58	179.51	0.163
17	0.287	171.73	1.70	39.15	179.91	0.029	338.73	179.51	0.152
18	0.199	161.92	1.73	25.94	179.63	0.027	250.23	179.53	0.150
19	0.110	170.78	3.13	14.59	-179.79	0.026	154.83	179.41	0.152
20	0.091	123.96	5.14	5.27	-179.60	0.022	63.66	178.03	0.183

Table G.10 Mode shapes, test H.

Point no.	1st mode			2nd mode			3rd mode		
	$|\phi_{1i}|$	Phase Deg.	Error	$|\phi_{2i}|$	Phase Deg.	Error	$|\phi_{3i}|$	Phase Deg	Error
1	4.58	-179.91	2.25	112.10	-0.73	0.050	451.64	179.79	0.120
2	4.42	-179.43	2.18	85.29	-0.46	0.047	273.74	-179.96	0.116
3	3.96	179.84	2.22	58.84	-0.16	0.042	88.92	179.73	0.096
4	3.65	-179.12	2.18	31.10	0.21	0.028	86.65	-0.34	0.163
5	3.40	-179.05	2.08	6.44	0.53	0.047	220.51	-0.53	0.140
6	3.08	179.06	2.04	16.41	179.35	0.160	308.31	-0.80	0.132
7	2.78	179.32	2.00	36.13	179.53	0.094	341.75	-0.74	0.124
8	2.42	-179.32	1.95	54.31	179.66	0.074	321.44	-0.06	0.112
9	2.18	179.85	1.91	68.06	179.21	0.066	251.52	-0.17	0.098
10	1.89	179.80	1.79	77.88	179.10	0.059	136.08	-0.10	0.066
11	1.63	-177.47	1.72	83.57	179.22	0.052	2.73	32.17	3.190
12	1.38	-179.47	1.60	84.33	179.00	0.046	138.36	178.13	0.205
13	1.12	179.92	1.52	81.11	178.77	0.042	261.17	179.03	0.158
14	0.909	178.91	1.37	74.90	178.83	0.038	351.82	179.31	0.142
15	0.715	179.16	1.19	64.78	178.94	0.034	395.11	179.40	0.132
16	0.515	177.36	1.12	51.96	178.79	0.033	389.52	178.52	0.131
17	0.384	173.93	1.20	40.21	178.93	0.028	342.46	178.50	0.123
18	0.251	174.43	1.56	27.76	178.94	0.025	263.55	178.40	0.118
19	0.149	164.85	2.16	15.27	179.34	0.020	161.02	179.15	0.128
20	0.069	151.24	6.53	5.50	179.12	0.022	65.88	177.33	0.157

Table G.11 Mode shapes, test I.

Point no.	1st mode			2nd mode			3rd mode		
	$|\phi_{1i}|$	Phase Deg.	Error	$|\phi_{2i}|$	Phase Deg.	Error	$|\phi_{3i}|$	Phase Deg	Error
1	4.58	179.77	2.44	110.94	-0.178	0.048	443.32	179.66	0.117
2	4.22	-179.98	2.45	84.74	-0.314	0.043	271.48	179.33	0.105
3	3.70	-179.75	2.46	58.07	-0.186	0.037	87.31	179.15	0.084
4	3.54	-178.31	2.35	31.77	-0.543	0.023	80.78	-1.35	0.156
5	3.29	178.81	2.33	6.64	0.255	0.047	217.25	-2.05	0.139
6	2.93	179.28	2.28	15.83	-179.92	0.167	301.02	-1.75	0.127
7	2.63	-177.97	2.22	36.09	179.94	0.092	333.21	-1.28	0.115
8	2.33	178.76	2.25	53.50	179.73	0.073	312.03	-1.31	0.104
9	2.16	178.95	2.08	66.68	179.7	0.064	246.02	-0.392	0.093
10	1.96	177.74	1.97	77.13	179.58	0.057	136.88	0.031	0.063
11	1.67	-178.88	1.88	82.49	179.49	0.051	5.88	11.58	2.310
12	1.45	-179.16	1.75	83.81	179.4	0.045	129.14	179.11	0.199
13	1.15	-177.61	1.65	80.90	179.23	0.040	255.85	179.32	0.150
14	0.876	179.86	1.53	74.52	179.27	0.036	338.82	179.58	0.135
15	0.704	178.80	1.37	65.42	179.3	0.032	384.74	179.58	0.128
16	0.504	179.23	1.19	52.21	179.33	0.032	376.52	179.42	0.126
17	0.324	176.14	1.02	39.78	179.49	0.028	328.98	179.38	0.120
18	0.242	175.56	0.768	27.30	179.56	0.027	250.34	179.50	0.120
19	0.140	-174.96	0.800	14.80	179.88	0.028	149.06	178.86	0.122
20	0.041	134.00	12.13	5.42	-179.86	0.031	64.60	177.02	0.138

Table G.12 Mode shapes, test J.

Point no.	1st mode			2nd mode			3rd mode		
	$|\phi_{1i}|$	Phase Deg.	Error	$|\phi_{2i}|$	Phase Deg.	Error	$|\phi_{3i}|$	Phase Deg	Error
1	4.50	179.83	5.94	111.06	-0.755	0.043	448.37	179.31	0.323
2	4.27	-178.21	5.81	85.75	-0.531	0.040	277.21	179.46	0.316
3	3.92	179.86	5.82	59.09	-0.216	0.035	94.03	179.59	0.284
4	3.53	-179.88	5.83	32.16	-0.433	0.023	79.57	-0.830	0.399
5	3.28	-179.51	5.72	7.75	-0.587	0.032	215.13	-0.599	0.364
6	3.05	-179.70	5.62	14.60	179.32	0.173	301.50	-0.802	0.344
7	2.68	179.60	5.54	35.30	179.47	0.094	334.86	-0.657	0.337
8	2.43	179.97	5.42	53.18	179.22	0.074	316.64	-0.751	0.326
9	2.18	-179.45	5.36	66.16	179.36	0.063	247.85	-0.758	0.302
10	1.92	-179.58	5.21	76.20	179.30	0.056	140.33	-0.399	0.251
11	1.65	-179.96	5.05	81.96	179.49	0.050	12.56	8.65	0.286
12	1.38	-179.68	4.84	83.58	179.28	0.043	123.65	178.24	0.491
13	1.16	178.63	4.72	81.25	179.07	0.037	247.77	179.07	0.409
14	0.939	177.98	4.48	75.14	179.04	0.032	333.81	179.14	0.383
15	0.748	176.97	4.23	66.19	178.90	0.028	380.61	179.38	0.373
16	0.487	-179.28	3.92	52.43	179.21	0.025	374.21	179.37	0.370
17	0.332	177.10	3.62	40.11	179.01	0.020	326.34	179.32	0.357
18	0.225	177.89	3.26	27.84	179.11	0.020	249.43	179.53	0.358
19	0.122	170.31	2.91	15.60	179.09	0.021	154.17	179.08	0.363
20	0.040	26.61	16.87	5.08	179.47	0.032	61.44	178.23	0.349

Table G.13 Mode shapes, test K.

Point no.	1st mode			2nd mode			3rd mode		
	$|\phi_{1i}|$	Phase Deg.	Error	$|\phi_{2i}|$	Phase Deg.	Error	$|\phi_{3i}|$	Phase Deg	Error
1	4.26	-179.29	5.94	112.71	-0.03	0.0360	446.46	179.68	0.132
2	4.04	179.01	5.81	86.07	-0.16	0.0336	275.51	179.83	0.126
3	3.76	-178.64	5.82	59.88	-0.10	0.0283	93.32	179.61	0.104
4	3.42	178.06	5.83	33.83	0.10	0.0178	72.88	0.386	0.166
5	3.38	175.48	5.72	10.14	-1.20	0.0125	201.57	- 0.098	0.140
6	2.90	179.16	5.62	12.49	179.57	0.1809	290.59	- 0.473	0.133
7	2.62	-177.29	5.54	32.62	179.47	0.0802	324.8	-0.268	0.125
8	2.43	179.14	5.42	49.44	179.43	0.0612	311.24	0.168	0.117
9	2.09	-177.96	5.36	64.03	179.71	0.0515	248.4	0.138	0.107
10	1.86	-178.89	5.21	74.58	179.73	0.0445	137.01	0.448	0.078
11	1.64	-179.94	5.05	80.65	179.58	0.0392	15.36	6.01	0.246
12	1.37	-179.66	4.84	82.91	179.36	0.0341	118.11	178.43	0.223
13	1.17	179.73	4.72	80.68	179.36	0.0293	239.11	179.27	0.170
14	0.98	179.30	4.48	75.70	179.26	0.0252	318.67	179.39	0.163
15	0.78	-179.62	4.23	67.04	179.25	0.0209	371.26	179.35	0.154
16	0.58	178.66	3.92	53.99	179.18	0.0187	367.32	179.37	0.150
17	0.39	-175.74	3.62	41.66	179.27	0.0142	322.33	179.41	0.142
18	0.30	178.94	3.26	30.85	179.22	0.0126	260.15	179.29	0.139
19	0.11	-171.72	2.91	16.17	179.18	0.0110	151.36	178.06	0.133
20	0.04	-144.46	16.87	5.35	178.86	0.0103	61.94	176.42	0.120

A. RYTTER ET AL.

Table G.14 Mode shapes, test L.

Point no.	1st mode			2nd mode			3rd mode		
	$|\mathfrak{e}_{1i}|$	Phase Deg.	Error	$|\mathfrak{e}_{2i}|$	Phase Deg.	Error	$|\mathfrak{e}_{3i}|$	Phase Deg	Error
1	3.57	179.34	3.18	106.20	1.26	0.072	429.77	-178.35	0.170
2	3.48	178.09	3.10	83.68	1.50	0.083	271.62	-178.04	0.179
3	3.35	177.39	3.01	59.79	1.51	0.067	95.72	-177.76	0.164
4	3.06	177.36	3.04	34.63	1.97	0.077	73.02	3.58	0.243
5	2.72	179.62	3.02	11.02	2.16	0.073	202.27	2.57	0.207
6	2.57	178.02	2.92	10.43	-177.85	0.287	288.51	1.89	0.176
7	2.30	178.60	2.90	29.42	-178.60	0.131	323.46	1.79	0.166
8	2.21	177.36	2.78	45.67	-178.15	0.127	314.74	2.27	0.170
9	1.99	177.70	2.70	59.53	-178.60	0.112	256.00	1.95	0.154
10	1.74	177.47	2.65	69.41	-179.01	0.082	150.51	2.24	0.117
11	1.52	177.64	2.56	75.18	-179.24	0.063	29.44	7.68	0.196
12	1.35	178.43	2.37	79.47	-178.65	0.081	97.96	-179.44	0.300
13	1.16	175.91	2.27	78.64	-179.24	0.069	221.20	-179.45	0.213
14	0.915	176.93	2.18	73.71	-179.85	0.055	309.64	-179.68	0.182
15	0.774	176.58	2.02	65.65	179.63	0.049	358.68	-179.81	0.167
16	0.576	175.05	2.80	53.16	179.53	0.030	357.75	-179.78	0.150
17	0.438	168.91	2.88	41.82	179.44	0.023	320.95	-179.45	0.137
18	0.283	163.69	2.01	29.27	179.27	0.018	247.66	-179.73	0.131
19	0.190	171.44	2.40	15.65	178.79	0.016	145.20	179.46	0.130
20	0.093	-154.85	7.05	4.70	179.95	0.029	55.03	-179.36	0.145

APPENDIX H
TEST RESULTS, Beam no. 6

Table H.1 Crack lengths

Test	Crack length		
	Left mm	Right mm	Total mm
A	0	0	0.00
B	10.0	10.0	20.0
C	19.4	18.3	37.7
D	25.5	23.3	48.8
E	30.8	27.7	58.5
F	35.2	28.4	63.6
G	38.8	30.3	69.1
H	53.6	33.2	86.8
I	71.3	39.7	111.0
J	74.3	58.6	132.9

A. RYTTER ET AL.

Table H.2 Natural frequencies.

TEST	1st mode		2nd mode		3rd mode		4th mode	
	f Hz	σ_f Hz	f Hz	σ_f Hz	f Hz	BW Hz	f Hz	BW Hz
A	11.378	2.44e-05	71.074	6.385e-04	191.6	0.04	-	-
B	11.409	2.673e-05	71.054	6.063e-04	191.1	0.1	352	2
C	11.31	2.439e-05	70.671	3.344e-04	190.5	0.1	351	2
D	11.222	2.445e-05	70.35	2.950e-04	189.9	0.1	351	2
E	11.053	2.721e-05	69.749	1.782e-04	189.2	0.1	350	2
F	10.963	2.788e-05	69.454	1.188e-04	188.5	0.1	350	2
G	10.819	2.425e-05	68.963	1.800e-04	187.8	0.1	349	2
H	9.9721	2.383e-05	66.629	2.312e-04	185.1	0.1	347	2
I	8.1006	1.543e-04	63.609	4.099e-04	181.9	0.1	347	2
J	5.328	1.257e-4	58.86	5.449e-4	176.22	0.1	347	2

Table H.3 Natural frequencies. Lumped mass included.

TEST	1st mode		2nd mode		3rd mode		4th mode	
	f Hz	σ_f Hz	f Hz	σ_f Hz	f Hz	BW Hz	f Hz	BW Hz
B_m1	11.135	2.902e-05	69.554	1.196e-03	185.9	0.1	0	2
B_m2	11.401	3.068e-05	70.78	8.771e-04	187.7	0.1	0	2
E_m1	10.786	0.000	68.4	0.000	183.8	0.1	352	2
E_m2	11.047	2.656e-05	69.429	1.611e-04	185.6	0.1	344	2

Table H.4 Modal damping ratios.

TEST	1st mode		2nd mode	
	ζ	σ_ζ	ζ	σ_ζ
A	7.750e-04	2.140e-06	0.202e-03	8.98e-06
B	4.989e-04	2.342e-06	1.507e-03	8.537e-06
C	5.712e-04	2.168e-06	1.310e-03	4.727e-06
D	5.738e-04	2.152e-06	1.244e-03	4.188e-06
E	6.570e-04	2.458e-06	1.055e-03	2.552e-06
F	7.153e-04	2.585e-06	7.474e-04	1.711e-06
G	8.828e-04	2.224e-06	1.069e-03	2.611e-06
H	1.996e-03	2.401e-06	1.096e-03	3.470e-06
I	1.574e-03	1.901e-05	9.064e-04	6.444e-06
J	6.035e-03	2.327e-05	2.771e-03	9.246e-06

Table H.5 Modal damping ratios. Lumped mass included.

TEST	1st mode		2nd mode	
	ζ	σ_ζ	ζ	σ_ζ
B_m1	5.428e-04	2.609e-06	1.243e-03	1.719e-05
B_m2	6.230e-04	2.694e-06	1.330e-03	1.240e-05
E_m1	6.290e-04	0.000	0.000	0.000
E_m2	7.065e-04	2.413e-06	9.729e-04	2.318e-06

A. RYTTER ET AL.

Table H.6 Mode shape ratios.

TEST	1st mode				2nd mode			
	Φ_2/Φ_1		Φ_3/Φ_1		Φ_2/Φ_1		Φ_3/Φ_1	
	Est.	σ	Est.	σ	Est.	σ	Est.	σ
A	0.6517	2.202e-4	0.097	9.11e-05	-	-	-	-
B	0.597	2.227e-0	0.100	8.944e-0	-0.364	4.171e-0	-0.446	2.806e-0
C	0.607	2.062e-0	0.103	9.134e-0	-0.369	2.117e-0	-0.462	1.764e-0
D	0.608	2.017e-0	0.104	1.037e-0	-0.354	1.849e-0	-0.465	1.615e-0
E	0.611	2.298e-0	0.105	9.123e-0	-0.362	1.153e-0	-0.463	1.013e-0
F	0.612	2.377e-0	0.109	1.228e-0	-0.359	7.828e-0	-0.468	8.571e-0
G	0.615	2.045e-0	0.112	1.126e-0	-0.349	1.249e-0	-0.471	1.071e-0
H	0.624	2.009e-0	0.125	1.356e-0	-0.331	1.307e-0	-0.489	1.468e-0
I	0.648	1.639e-0	0.156	3.900e-0	-0.108	1.927e-0	-0.514	2.953e-0
J	0.671	1.070e-0	0.187	5.949e-0	-0.248	2.374e-0	-0.515	2.520e-0

Table H.7 Mode shape ratios. Lumped mass included.

TEST	1st mode				2nd mode			
	Φ_2/Φ_1		Φ_3/Φ_1		Φ_2/Φ_1		Φ_3/Φ_1	
	Est.	σ	Est.	σ	Est.	σ	Est.	σ
B_m1	0.605	2.413e-04	0.100	1.165e-04	-0.325	7.457e-03	-0.415	5.651e-03
B_m2	0.603	2.539e-04	0.099	1.362e-04	-0.370	5.161e-03	-0.452	4.931e-03
E_m1	0.629	0.000	0.106	0.000	0	0.000	0	0.000
E_m2	0.611	2.259e-04	0.106	1.102e-04	-0.361	1.084e-03	-0.460	9.502e-04

FRACTURE AND DYNAMICS PAPERS

PAPER NO. 8: P. H. Kirkegaard, I. Enevoldsen, J. D. Sørensen, R. Brincker: *Reliability Analysis of a Mono-Tower Platform*. ISSN 0902-7513 R8839.

PAPER NO. 9: P. H. Kirkegaard, J. D. Sørensen, R. Brincker: *Fatigue Analysis of a Mono-Tower Platform*. ISSN 0902-7513 R8840.

PAPER NO. 10: Jakob Laigaard Jensen: *System Identification1: ARMA Models*. ISSN 0902-7513 R8908.

PAPER NO. 11: Henrik Dahl & Rune Brincker: *Fracture Energy of High-Strength Concrete in Compression*. ISSN 0902-7513 R8919.

PAPER NO. 12: Lise Gansted, Rune Brincker & Lars Pilegaard Hansen: *Numerical Cumulative Damage: The FM-Model*. ISSN 0902-7513 R8920.

PAPER NO. 13: Lise Gansted: *Fatigue of Steel: Deterministic Loading on CT-Specimens*.

PAPER NO. 14: Jakob Laigaard Jensen, Rune Brincker & Anders Rytter: *Identification of Light Damping in Structures*. ISSN 0902-7513 R8928.

PAPER NO. 15: Anders Rytter, Jakob Laigaard Jensen & Lars Pilegaard Hansen: *System Identification from Output Measurements*. ISSN 0902-7513 R8929.

PAPER NO. 16: Jens Peder Ulfkjær: *Brud i beton - State-of-the-Art. 1. del, brudforløb og brudmodeller*. ISSN 0902-7513 R9001.

PAPER NO. 17: Jakob Laigaard Jensen: *Full-Scale Measurements of Offshore Platforms*. ISSN 0902-7513 R9002.

PAPER NO. 18: Jakob Laigaard Jensen, Rune Brincker & Anders Rytter: *Uncertainty of Modal Parameters Estimated by ARMA Models*. ISSN 0902-7513 R9006.

PAPER NO. 19: Rune Brincker: *Crack Tip Parameters for Growing Cracks in Linear Viscoelastic Materials*. ISSN 0902-7513 R9007.

PAPER NO. 20: Rune Brincker, Jakob L. Jensen & Steen Krenk: *Spectral Estimation by the Random Dec Technique*. ISSN 0902-7513 R9008.

PAPER NO. 21: P. H. Kirkegaard, J. D. Sørensen & Rune Brincker: *Optimization of Measurements on Dynamically Sensitive Structures Using a Reliability Approach*. ISSN 0902-7513 R9009.

PAPER NO. 22: Jakob Laigaard Jensen: *System Identification of Offshore Platforms*. ISSN 0902-7513 R9011.

PAPER NO. 23: Janus Lyngbye & Rune Brincker: *Crack Length Detection by Digital Image Processing*. ISSN 0902-7513 R9018.

PAPER NO 24: Jens Peder Ulfkjær, Rune Brinker & Steen Krenk: *Analytical Model for Complete Moment-Rotation Curves of Concrete Beams in bending*. ISSN 0902-7513 R9021.

FRACTURE AND DYNAMICS PAPERS

PAPER NO 25: Leo Thesbjerg: *Active Vibration Control of Civil Engineering Structures under Earthquake Excitation*. ISSN 0902-7513 R9027.

PAPER NO. 26: Rune Brincker, Steen Krenk & Jakob Laigaard Jensen: *Estimation of correlation Functions by the Random Dec Technique*. ISSN 0902-7513 R9028.

PAPER NO. 27: Jakob Laigaard Jensen, Poul Henning Kirkegaard & Rune Brincker: *Model and Wave Load Identification by ARMA Calibration*. ISSN 0902-7513 R9035.

PAPER NO. 28: Rune Brincker, Steen Krenk & Jakob Laigaard Jensen: *Estimation of Correlation Functions by the Random Decrement Technique*. ISSN 0902-7513 R9041.

PAPER NO. 29: Poul Henning Kirkegaard, John D. Sørensen & Rune Brincker: *Optimal Design of Measurement Programs for the Parameter Identification of Dynamic Systems*. ISSN 0902-7513 R9103.

PAPER NO. 30: L. Gansted & N. B. Sørensen: *Introduction to Fatigue and Fracture Mechanics*. ISSN 0902-7513 R9104.

PAPER NO. 31: R. Brincker, A. Rytter & S. Krenk: *Non-Parametric Estimation of Correlation Functions*. ISSN 0902-7513 R9120.

PAPER NO. 32: R. Brincker, P. H. Kirkegaard & A. Rytter: *Identification of System Parameters by the Random Decrement Technique*. ISSN 0902-7513 R9121.

PAPER NO. 33: A. Rytter, R. Brincker & L. Pilegaard Hansen: *Detection of Fatigue Damage in a Steel Member*. ISSN 0902-7513 R9138.

PAPER NO. 34: J. P. Ulfkjær, S. Krenk & R. Brincker: *Analytical Model for Fictitious Crack Propagation in Concrete Beams*. ISSN 0902-7513 R9206.

PAPER NO. 35: J. Lyngbye: *Applications of Digital Image Analysis in Experimental Mechanics*. Ph.D.-Thesis. ISSN 0902-7513 R9227.

PAPER NO. 36: J. P. Ulfkjær & R. Brincker: *Indirect Determination of the $\sigma - w$ Relation of HSC Through Three-Point Bending*. ISSN 0902-7513 R9229.

PAPER NO. 37: A. Rytter, R. Brincker & P. H. Kirkegaard: *An Experimental Study of the Modal Parameters of a Damaged Cantilever* ISSN 0902-7513 R9230.